# Conformational coupling of integrin and Thy-1 regulates Fyn priming and fibroblast mechanotransduction

Vincent F. Fiore,[1] Patrick W. Strane,[1] Anton V. Bryksin,[1] Eric S. White,[2] James S. Hagood,[3] and Thomas H. Barker[1,4]

[1]Wallace H. Coulter Department of Biomedical Engineering, Georgia Institute of Technology, Atlanta, GA 30332
[2]Division of Pulmonary and Critical Care Medicine, Department of Internal Medicine, University of Michigan, Ann Arbor, MI 48109
[3]Division of Respiratory Medicine, Department of Pediatrics, University of California, Rady Children's Hospital, San Diego, CA 92105
[4]Petit Institute for Bioengineering and Biosciences, Georgia Institute of Technology, Atlanta, GA 30332

Progressive fibrosis is characterized by excessive deposition of extracellular matrix (ECM), resulting in gross alterations in tissue mechanics. Changes in tissue mechanics can further augment scar deposition through fibroblast mechanotransduction. In idiopathic pulmonary fibrosis, a fatal form of progressive lung fibrosis, previous work has shown that loss of Thy-1 (CD90) expression in fibroblasts correlates with regions of active fibrogenesis, thus representing a pathologically relevant fibroblast subpopulation. We now show that Thy-1 is a regulator of fibroblast rigidity sensing. Thy-1 physically couples to inactive $\alpha_v\beta_3$ integrins via its RGD-like motif, altering baseline integrin avidity to ECM ligands and also facilitating preadhesion clustering of integrin and membrane rafts via Thy-1's glycophosphatidylinositol tether. Disruption of Thy-1–$\alpha_v\beta_3$ coupling altered recruitment of Src family kinases to adhesion complexes and impaired mechanosensitive, force-induced Rho signaling, and rigidity sensing. Loss of Thy-1 was sufficient to induce myofibroblast differentiation in soft ECMs and may represent a physiological mechanism important in wound healing and fibrosis.

## Introduction

Progressive fibrosis and the resulting disruption of organ function is a major cause of morbidity and mortality worldwide, with limited treatment options often necessitating organ transplantation (Hardie et al., 2009). Although fibroblasts are the primary cell type responsible for stromal maintenance and remodeling during normal tissue homeostasis and wound healing (Sorrell and Caplan, 2009), their persistent activation is typical of pathological fibrosis in multiple organs and in cancer (Tomasek et al., 2002; Butcher et al., 2009). In idiopathic pulmonary fibrosis (IPF), an incurable form of progressive lung fibrosis, fibroblasts accumulate within an interconnected reticulum of high synthetic and ECM remodeling activity, termed fibroblastic foci (Cool et al., 2006), which is the histological feature most highly correlated with disease progression and patient morbidity (King et al., 2001; Nicholson et al., 2002). Fibroblasts are also extremely sensitive to the mechanics of their microenvironment, which is grossly altered during fibrotic progression. Work from our laboratory and others has quantified the microscale rigidity of lung tissue, demonstrating focal and large-magnitude increases in tissue and ECM stiffness as a result of IPF pathogenesis; the Young's modulus (i.e., rigidity, $E$) of normal and fibrotic lung tissue is 0.5–5 and 1–100 kPa, respectively (Liu et al., 2010; Booth et al., 2012; Brown et al., 2013). This has led to the hypothesis that aberrant tissue stiffness drives fibrotic responses. Supporting this notion, stiff ECM promotes actomyosin contractility, maturation of the actin cytoskeleton and associated focal adhesions (FAs), and ECM assembly/remodeling (Yeung et al., 2005; Wipff et al., 2007; Liu et al., 2010). Increased ECM stiffness also stimulates fibroblast activation of latent transforming growth factor β (Wipff et al., 2007), myofibroblast differentiation (Goffin et al., 2006; Huang et al., 2012), and epithelial to mesenchymal transition (Markowski et al., 2012; Brown et al., 2013), cellular changes associated with disease progression. Despite this correlation between fibrotic progression and stiffness-associated cell responses, the extent to which dynamic reciprocity between the mechanical microenvironment and cell-intrinsic adaptations initiate or perpetuate progressive fibrosis is poorly understood.

Fibroblasts also display marked phenotypic heterogeneity (Chang et al., 2002; Sorrell and Caplan, 2004), which is exacerbated in fibrotic diseases such as IPF because of the spatial and

The Rockefeller University Press $30.00
J. Cell Biol. Vol. 211 No. 1 173–190
www.jcb.org/cgi/doi/10.1083/jcb.201505007

JCB 173

temporal diversity of disease presentation, e.g., the intermixture of normal lung parenchyma, new fibrotic tissue (i.e., fibroblastic foci), mature fibrosis, and cystic "honeycomb" features within biopsied tissue segments (Visscher and Myers, 2006). Our work has previously demonstrated that fibroblasts within fibroblastic foci lack expression of the cell-surface glycoprotein Thy-1, whereas fibroblasts in normal lung interstitium are Thy-1 positive (Thy-1^{pos}; Hagood et al., 2005; Sanders et al., 2008). Thy-1 expression in lung fibroblasts (LFs) is transiently downregulated by Th1-type cytokines and chronically in IPF by epigenetic silencing (Hagood et al., 2005; Sanders et al., 2008; Bradley et al., 2013). Furthermore, Thy-1 expression decreases in aging lungs associated with abnormal ECM (Sueblinvong et al., 2012), and we have shown that genetic loss of Thy-1 in mice consistently results in more severe fibrosis, suggesting that persistent Thy-1 loss is pathologically relevant to disease progression (Hagood et al., 2005). Thy-1, also known as CD90, is a small glycophosphatidylinositol (GPI)-anchored glycoprotein that alters fibroblast phenotype through modulating Src family kinase (SFK) and Rho GTPase intracellular signaling pathways through unknown mechanisms (Barker and Hagood, 2009). It remains unclear how Thy-1, tethered to the outer leaflet of the plasma membrane via its GPI linkage, modulates intracellular signaling. Nevertheless, Thy-1 surface expression is sufficient to alter basal SFK activation, p190 RhoGAP phosphorylation, and downstream Rho signaling, leading to differential FA and stress fiber formation and migration on rigid (i.e., glass) surfaces (Barker et al., 2004a,b; Rege et al., 2006). However, the effect of Thy-1 on fibroblast adaptation to fibrosis-associated extrinsic cues, such as increased ECM stiffness, and the molecular mechanism(s) by which Thy-1 exerts its effects on signaling and downstream fibroblast phenotypes are unknown.

Transduction of mechanical signals into cell phenotypes is critical in complex disease pathologies where the mechanical environment of the affected cells is dynamic and heterogeneous. As the macromolecular complex of structural and signaling proteins linking the ECM to the cytoskeleton, integrin-based adhesion complexes (i.e., FAs) are the primary sites of cell–ECM force transmission and are capable of transducing such forces into biochemical signals (i.e., mechanotransduction; Hoffman et al., 2011; Wolfenson et al., 2013). How these proteins associate in space and time is critical for FA function, although less well understood are processes regulating FA assembly and mechanosignaling that act upstream of integrin-ECM binding. Preceding immobilization, integrins exhibit lateral mobility (Duband et al., 1988; Wiseman et al., 2004) within the plasma membrane before becoming kinetically trapped within regions of close proximity to the substratum and enhanced probability of ligand association (Paszek et al., 2009, 2014). Even within FA structures, integrins are highly mobile, exhibiting intermittent modes of confinement, diffusion, and immobilization depending on their tripartite interaction with the ECM and the cytoskeleton (Rossier et al., 2012). Furthermore, simply clustering integrins in the absence of ligation or force recruits downstream signaling molecules requisite for early ligand-induced signal generation, such as SFKs (Shattil, 2005; Boettiger, 2012). Intriguingly, not all early signaling intermediates directly bind to integrin receptors, necessitating alternate scaffolding molecules to bridge these interactions. In support of this view, cis-binding integrin regulatory molecules have been identified (Lindberg et al., 1996; Wei et al., 1996, 2005; Watanabe and Sendo, 2002);

however, their mechanisms of action and downstream biological consequences are not fully understood.

Motivated by the strong correlation of Thy-1 loss with regions of active fibrotic remodeling in IPF, we now show that Thy-1 is a novel regulator of fibroblast mechanotransduction. Thy-1 elicits these responses through multiple activities emanating from its ability to bind inactive integrin in the plane of the membrane. First, Thy-1 binding to integrin alters its baseline avidity to ECM ligands. Second, Thy-1 facilitates the recruitment of membrane raft-residing signaling molecules such as Fyn kinase and the SFK regulator, Csk binding protein (Cbp), to FAs via its direct coupling of integrins and raft domains. Loss of Thy-1 results in elevated cytoskeletal activation and myofibroblast phenotypes in soft, physiological ECMs and constitutively active SFK signaling from FAs.

## Results

### Thy-1 confers mechanosensitive cytoskeletal remodeling to changes in ECM rigidity

To study the role of Thy-1 expression on the mechanotransductory phenotype of LFs, we isolated primary LFs from adult mice and used FACS to generate Thy-1^{pos} and Thy-1–negative (Thy-1^{neg}) subpopulations (Fig. 1 a). To isolate rigidity-specific responses, we cultured cells on fibronectin-coated polyacrylamide (FN-PA) substrates of controlled rigidity (Young's modulus, $E$) from 1 to 20 kPa, a range spanning normal alveolar interstitium to pathological fibrosis. In response to increasing substrate rigidity, Thy-1^{pos} mouse lung fibroblasts (MLFs) exhibited pronounced cytoskeletal reorganization, including the assembly of actin stress fibers and large FAs typical of physiological rigidity sensing (Fig. 1 b). Cortical stiffness (a direct quantification of cytoskeletal organization and contractile activity) increased approximately fourfold from softest (1.8 kPa) to stiffest (18.7 kPa) substrates, effectively saturating responses at the higher value. Cell area and FA size also monotonically increased with substrate $E$ in Thy-1^{pos} fibroblasts (Fig. 1 d and Fig. S1), consistent with previous studies of fibroblast rigidity sensing (Pelham and Wang, 1997; Solon et al., 2007). Strikingly, Thy-1^{neg} fibroblasts had more pronounced stress fibers and increased cortical stiffness and FA size on soft substrates and a significantly muted sensitivity to increasing substrate rigidity (Fig. 1, b–d; and Fig. S1). To explore a specific role for Thy-1, we expressed wild-type Thy-1 (Thy-1[WT]) at endogenous levels or an empty vector control in the Thy-1^{neg} LF line RFL-6. Thy-1[WT] reexpression largely recapitulated the rigidity-dependent cytoskeletal phenotypes of cortical stiffening, cell spreading and FA assembly observed in endogenous FACS-sorted subpopulations (Fig. 1, b–d). We have previously shown that Thy-1 expression elevates basal fibroblast activity of RhoA on stiff ($E \sim 3$ GPa) glass substrates (Barker et al., 2004a). Here, empty vector control RFL-6 exhibited muted activation of RhoA when cultured on increasing substrate $E$, whereas in Thy-1[WT] RFL-6, RhoA activity robustly and sensitively correlated with substrate $E$ and cytoskeletal remodeling (i.e., cell spreading, cortical stiffness; Fig. 1 e). These findings suggest that Thy-1–dependent processes modulate the activity state of RhoA to control rigidity-dependent cytoskeletal remodeling and FA assembly.
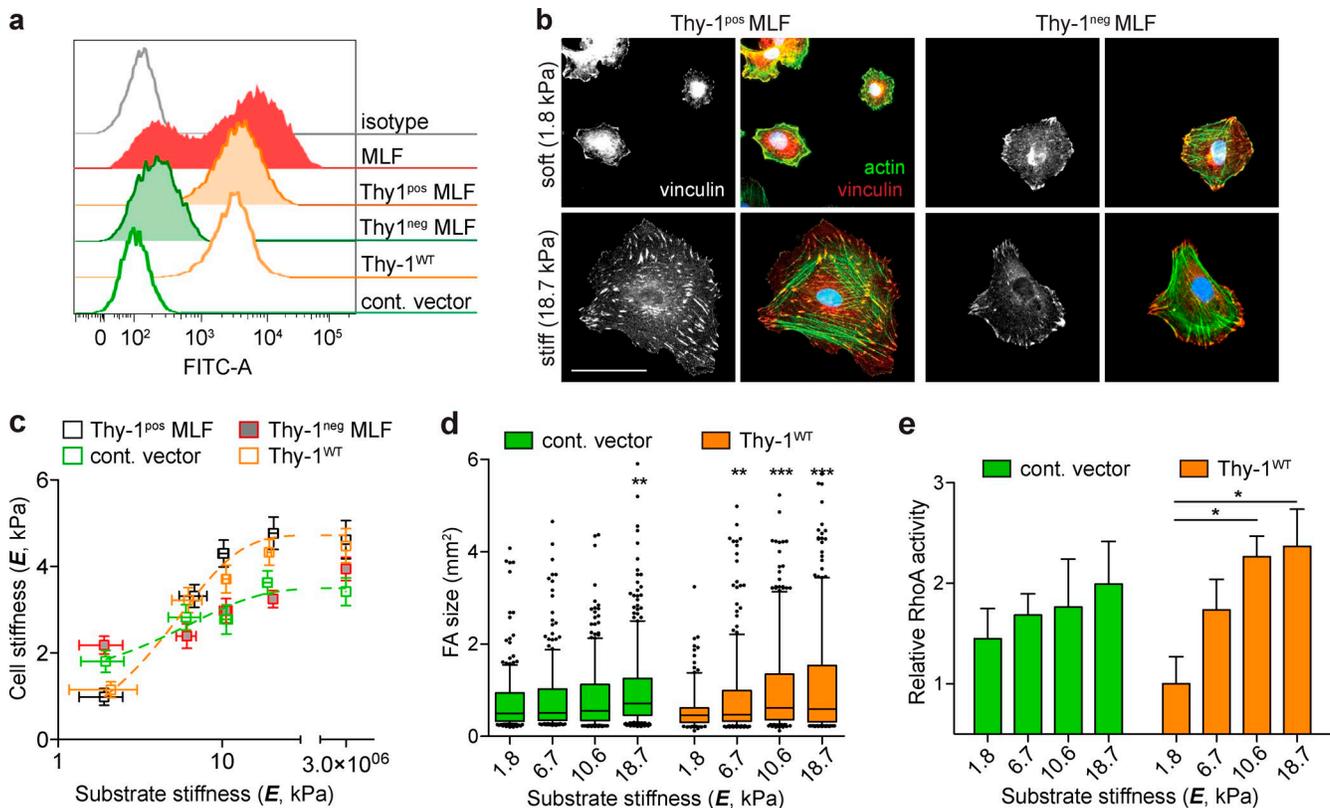
Figure 1. **Thy-1 confers mechanosensitive cytoskeletal remodeling to changes in ECM rigidity.** (a) FACS analysis demonstrates heterogeneous Thy-1 expression in LFs. Primary MLFs were sorted for Thy-1 expression into Thy-1$^{pos}$ and Thy-1$^{neg}$ subpopulations, and the RFL-6 cell line stably expressing Thy-1$^{WT}$ or an empty vector control (cont. vector) was used. The data shown are from a single representative experiment out of more than five independent repeats. (b) Thy-1$^{pos}$ and Thy-1$^{neg}$ primary MLFs were plated on soft (1.8 kPa) or stiff (18.7 kPa) FN-PA substrates for 4 h and immunostained for vinculin (left, grayscale; red, overlay) and F-actin (green, overlay). Bar, 50 µm. (c) Single-cell cortical stiffness measurements were made of Thy-1$^{pos}$ and Thy-1$^{neg}$ primary MLFs and cont. vector– and Thy-1$^{WT}$–expressing RFL-6 cells on FN-PA substrates of varying stiffness. n = 20–29 individual cells per individual data point (mean ± SEM). Data are pooled from three independent experiments. (d) FA size was measured under the same conditions; box-and-whisker plots (10th–90th percentiles with outlier points shown) of individual FA sizes for control vector– and Thy-1$^{WT}$–expressing RFL-6 cells is shown. A minimum of n = 12 cells from two independent experiments are shown. Statistical significance was calculated using the Kruskal-Wallis nonparametric test with Dunn's multiple comparisons. (e) Control vector– and Thy-1$^{WT}$–expressing RFL-6 cells were plated on FN-PA substrates of varying stiffness for 4 h and RhoA activity was measured using G-LISA assay (n = 5). One representative of two independent experiments is shown. One-way analysis of variance and Tukey's post hoc test were used to calculate statistical significance. *, P < 0.05; **, P < 0.01; ***, P < 0.001 between indicated groups.

## Thy-1 modulates force-dependent SFK and RhoA adhesion signaling

To directly test force-dependent FA signal transduction, we applied prescribed forces to FN-coated magnetic beads interacting with fibroblasts (Fig. 2 a). Consistent with previous studies (Guilluy et al., 2011), tensional forces applied across FN-integrin clusters activated RhoA, whereas application of force via the transferrin receptor did not (Fig. 2 b). In the presence of Thy-1, force application elevated the active RhoA levels approximately twofold after 5 min of force application (apparent rate constant $K = 1.42 ± 0.40$ min$^{-1}$, mean ± SEM), whereas in the absence of Thy-1 (empty vector control RFL-6), the activation rate ($K = 0.58 ± 0.28$) decreased and the plateau amplitude of RhoA activity was significantly repressed.

We subsequently isolated and analyzed the adhesion complexes associated with the FN-coated magnetic beads either before or after 3 min of constant force application. A candidate screen for known FA components revealed that α5 integrin subunits, talin, and paxillin were not differentially associated with the fibronectin (FN) adhesion complex before or after force application (Fig. 2, c and d). Focal adhesion kinase (FAK) was significantly activated in response to force in a Thy-1–

independent manner, consistent with previous studies on its role in mechanotransduction (Friedland et al., 2009; Guilluy et al., 2011). However, in the absence of Thy-1, FAK activity appeared slightly elevated in FAs before force application (Fig. 2, c and d), suggesting dysregulated basal FAK activation. As previously demonstrated, force application to the FA significantly increased SFK activity (i.e., pY418-SFK), but only in the presence of Thy-1$^{WT}$. In the absence of Thy-1, SFK displayed moderately high and constant activity levels regardless of force activation (Fig. 2, c and d), again suggesting a dysregulation of FA signaling. The presence of c-Src within FAs was not significantly dependent on Thy-1 expression or force application. However, recruitment of the SFK member Fyn to FAs was critically dependent on Thy-1 expression but not on force (Fig. 2, c and d). In the absence of Fyn, Thy-1–dependent force activation of SFKs was significantly muted, suggesting a prominent role for Fyn activation in response to tensional forces. These data suggest that Thy-1 affects both a force-dependent and independent (i.e., basal) activity of SFKs during adhesion to FN, and the recruitment of Fyn to FN-engaged FAs. Further supporting this interpretation, both Thy-1 and Fyn expression were required for rigidity sensing in c-Src/Yes/Fyn
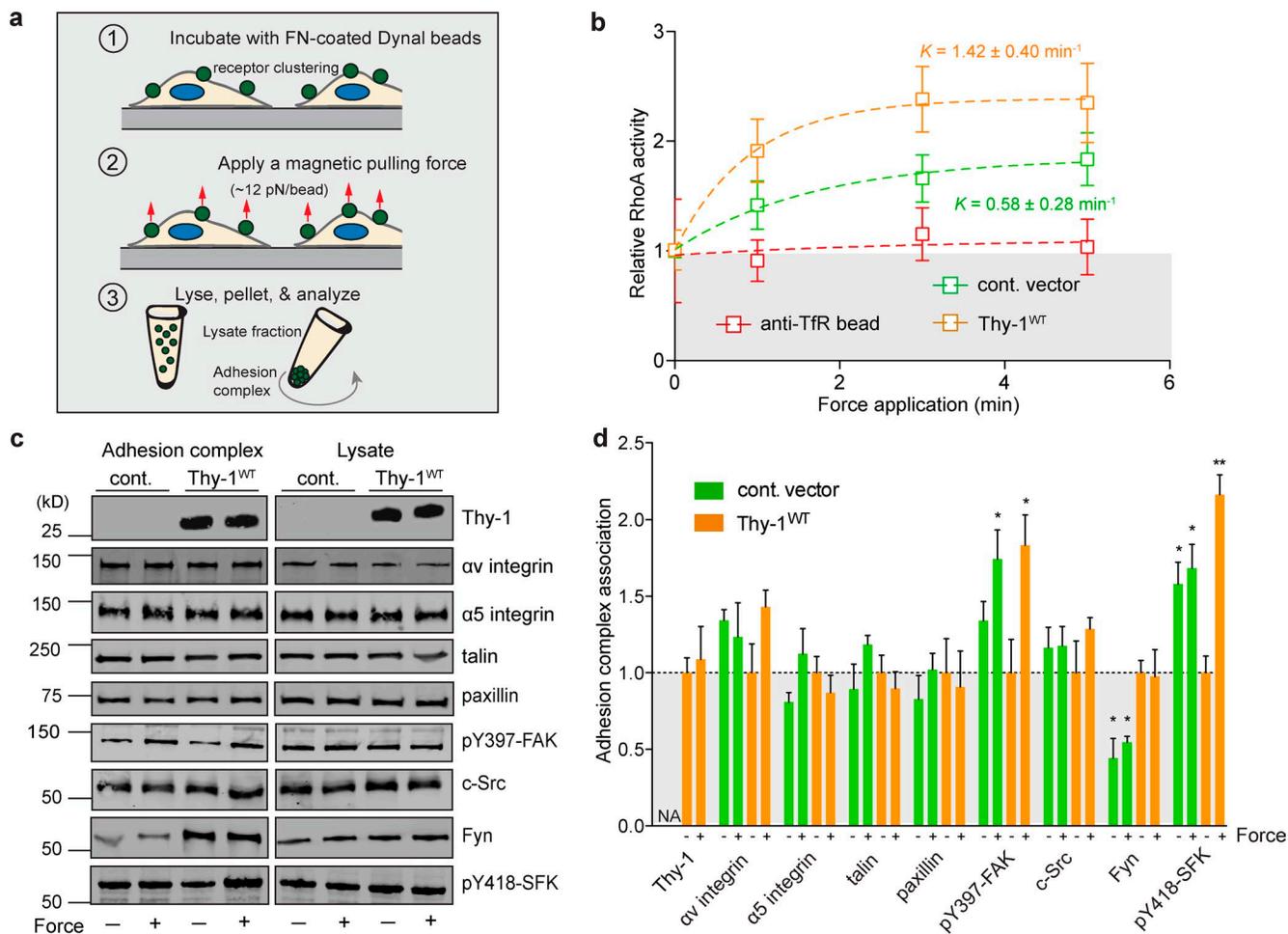
Figure 2. **Thy-1 modulates force-dependent SFK and RhoA adhesion signaling.** (a) Cartoon schematic of the tensile force application assay. Magnetic beads coated with FN are allowed to bind cell surface receptors, after which a permanent magnet is used to apply tensile force for varying amounts of time. Cells are then lysed for biochemical analysis. (b) RhoA activity was measured after tensile magnetic force stimulation of FN- or anti-transferrin receptor beads bound to empty vector control (cont. vector)– and Thy-1$^{WT}$–expressing RFL-6 cells. Apparent rate constants ($K$) for a single-phase association model are indicated (mean ± SEM); plateau phase of control vector was statistically different from Thy-1$^{WT}$ ($n$ = 6 biological replicates from two independent experiments; unpaired $t$ test, $P < 0.05$). Normalized baseline level for zero force is indicated in gray. TfR indicates transferrin receptor. (c) Immunoblots of FA proteins bound to FN beads (adhesion complex) before (− force) or after (+ force) 3 min of constant force application or total cell lysates in control vector and Thy-1$^{WT}$ RFL-6 cells are shown. (d) Immunoblots were quantified for $n$ = 3–4 biological replicates from two independent experiments for association to FN-bead adhesion complexes before (− force) or after (+ force). Significance was calculated between all groups for individual adhesion components using one-way analysis of variance and Tukey's post test. *, $P < 0.05$; **, $P < 0.01$ between indicated groups.

(SYF) triple knockout fibroblasts. c-Src expression alone, in both the presence and absence of Thy-1, did not enable rigidity sensing (Fig. S2, a and b).

**Membrane raft recruitment to FAs is facilitated by Thy-1 and participates in rigidity sensing**

Thy-1, through its GPI anchor, is known to associate with dually acylated SFKs, including Fyn, within membrane rafts and modulate their signaling activity (Stefanová et al., 1991; Dráberová and Dráber, 1993). We therefore explored the hypothesis that Thy-1 directly facilitates integrin-mediated recruitment of membrane raft–associated Fyn to FAs independent of force. Further supporting this hypothesis, Thy-1 additionally facilitated force-independent recruitment of other raft-associated molecules to FAs, including flotillin-2 and Cbp (Fig. 3 a). Disruption of membrane rafts with cholesterol oxidase (CholOx) dramatically inhibited Thy-1–associated recruitment of Fyn and

Cbp to FAs (Fig. 3 b) and Thy-1–dependent RhoA activation in response to force (Fig. S2 c). Furthermore, FA localization of membrane rafts marked by GM1 was decreased in the absence of Thy-1 (Fig. 3, c and d); however, total membrane GM1 staining was not different (Fig. S2, d and e). Thy-1–dependent GM1 localization was disrupted by membrane cholesterol perturbation (Fig. 3, c and d). To further explore the necessity of Thy-1's membrane raft association for Fyn recruitment, we substituted the endogenous GPI anchor of Thy-1 with the transmembrane domain of CD8 (Thy-1$^{/CD8}$). This mutation alters the localization of the Thy-1 ectodomain from its endogenous membrane raft sites (Tiveron et al., 1994). Using this construct we confirmed that Thy-1's GPI anchor and membrane raft localization is critical for Fyn recruitment to the FA and force-dependent SFK and RhoA activation (Fig. 3, e and f). The Thy-1$^{/CD8}$ mutant largely phenocopied the Thy-1$^{neg}$ phenotypes with respect to rigidity-sensitive cortical stiffening and FA formation (Fig. 3, g–i), however soft ECM phenotypes and elevated force-independent
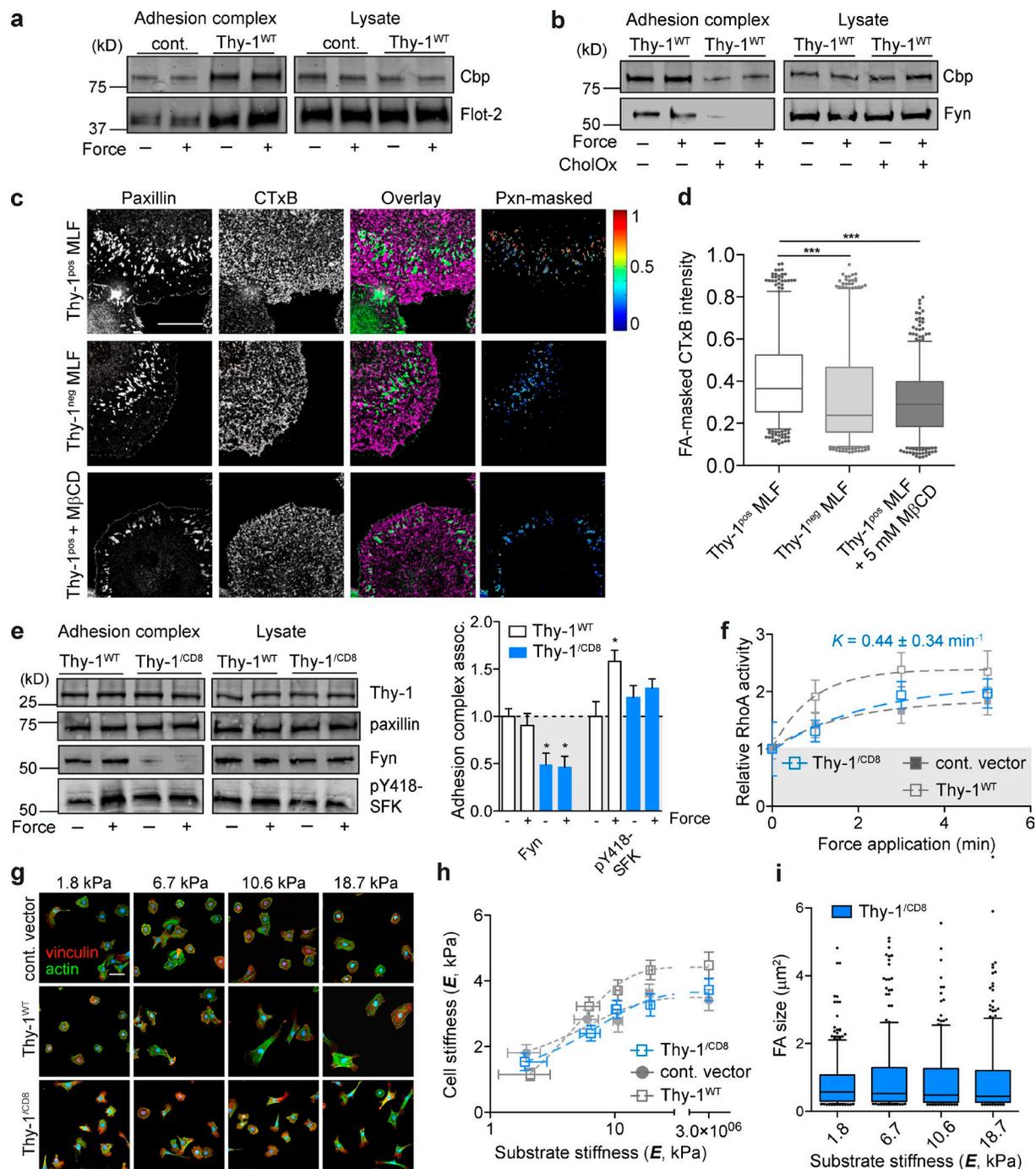
Figure 3. **Membrane raft recruitment to FAs is facilitated by Thy-1 and participates in rigidity sensing.** (a) Immunoblots of proteins associated with adhesion complex or total lysate before (− force) or after (+ force) 3-min force application in control vector and Thy-1[WT] RFL-6 cells. (b) Immunoblots as in (a) with or without 1 U/ml CholOx Thy-1[WT] RFL-6 cells. (c) Fluorescence images of MLFs on FN-coated glass (FN-gl) stained for paxillin (pxn) and membrane raft marker GM1 (CTxB), and FA (pxn)–masked CTxB intensity images are shown; the range of intensity values (arbitrary units) is indicated by heat scale. Bar, 50 µm. (d) Intensity of CTxB was quantified within paxillin-masked FAs (>2,500 FAs pooled for $n$ = 10–12 individual cells per group) for MLFs subpopulations and Thy1^{pos} treated with 5 mM MβCD. Significance was calculated using the Kruskal-Wallis nonparametric test with Dunn's multiple comparisons. (e) Immunoblots of proteins associated with FN beads before (− force) or after (+ force) 3 min of constant force application or total cell lysates in Thy-1[WT] and Thy-1[/CD8] RFL-6 cells. Averages of $n$ = 3 independent experiments for association with FN-bead adhesion complexes before (− force) or after 3-min force application (+ force). Significance was calculated between all groups for individual adhesion components using one-way analysis of variance and Tukey's post test. (f) Activation of RhoA after magnetic force stimulation of FN beads for the indicated time periods in Thy-1[/CD8] RFL-6 cells ($n$ = 5). Apparent rate constant ($K$) for a single-phase association model is indicated. Immunostaining for FAs and F-actin (g), single-cell cortical stiffness measurements (h), and FA quantification (i) of RFL-6 cells on FN-PA substrates of varying stiffness. Bar, 50 µm. *, P < 0.05; ***, P < 0.001 between indicated groups.

SFK activity were not as exaggerated compared with empty vector control RFL-6s. Together, these data strongly suggest that Thy-1's localization to membrane rafts and the stability of these domains are critical for the function of Thy-1 in physiological mechanotransduction and rigidity sensing.

### Thy-1 binds inactive $\alpha_v\beta_3$ integrin in cis, enabling integrin-mediated membrane raft recruitment to FAs

Thy-1 is known to support integrin-mediated transcellular adhesion in a variety of tissue-specific contexts via $\alpha_v\beta_3$ (Leyton et al., 2001; Saalbach et al., 2005; Hermosilla et al., 2008), $\alpha_v\beta_5$ (Zhou et al., 2010), and $\alpha_5\beta_1$ (Fiore et al., 2014). We found that Thy-1 coimmunoprecipitates with $\alpha_v$ integrins in conditions that discourage cell-cell interactions and in greater amounts in the absence of cell-matrix adhesion (i.e., suspension; Fig. 4 a). We further verified physical complexes between Thy-1 and integrin in situ using a proximity-based ligation assay (PLA). Integrins exist in multiple conformations that control ECM ligand affinity. In their low-affinity or inactive state, multiple integrins, including $\alpha_v\beta_3$, exhibit a "bent" conformation with their ligand-binding headpiece proximal to the plasma membrane (Xiong et al., 2001; Luo et al., 2007). Integrin activation extends the headpiece ~20 nm from the cell surface and facilitates high-affinity interactions with ligand (Takagi et al., 2002; Luo et al., 2007). We observed a PLA-positive signal only with antibodies that bind inhibiting (LM609; Lin et al., 1998) or nonfunctional (23C6; Byron et al., 2009) $\alpha_v\beta_3$ epitopes (Fig. S3), but not those that cooperatively bind (LIBS2; Du et al., 1993) or report the extended, active conformation (WOW-1; Pampori et al., 1999). We additionally observed positive PLA signal with nonconformation specific anti-$\beta_1$ antibodies, but not with those that report the extended conformation. No significant PLA was observed with $\alpha_5$ integrins (Fig. S3).

To examine the hypothesis that lateral association between Thy-1 and $\alpha_v\beta_3$ is preferential for integrins not in the high-affinity or extended conformation, we tested whether directly perturbing integrin conformation would influence the proximity of $\alpha_v\beta_3$ and Thy-1 as detected by PLA. Activation of integrin with $Mn^{2+}$ or overexpressing the head domain of talin (THD; Bouaouina et al., 2008), significantly diminished the PLA signal between anti–Thy-1 and nonfunctional anti-$\alpha_v\beta_3$ antibodies (Fig. 4 b). Furthermore, Thy-1–$\alpha_v\beta_3$ integrin complexes were observed predominantly outside of FAs (Fig. 4 c) strongly suggesting that Thy-1 forms a complex with "inactive," bent $\alpha_v\beta_3$ integrin upstream of canonical ECM-binding FAs and that ligation of ECM ligands, presumably by the high-affinity receptor, disrupts Thy-1–integrin coupling. Binding to $\alpha_v$ integrins and $\alpha_5\beta_1$ in trans (i.e., cell-cell interactions) has been shown to be direct and mediated by Thy-1's RGD-like motif, Arg-Leu-Asp (RLD), as mutation to nonfunctional Arg-Leu-Glu (RLE) abolishes binding (Hermosilla et al., 2008; Fiore et al., 2014). To test if the interaction reported by PLA was dependent on this integrin-binding motif within Thy-1, we expressed both wild-type (Thy-$1^{WT}$) and the RLD mutant (Thy-$1^{D37E}$) in CHO.B2 cells expressing human $\alpha_v$ and $\beta_3$ integrin subunits. Indeed, mutation of the RLD motif abolished PLA between Thy-1 and $\alpha_v\beta_3$ (Fig. 4 d). Interestingly, the binding of the GPI anchor mutant Thy-1 (Thy-$1^{/CD8}$) and $\alpha_v\beta_3$ was also diminished but not completely abrogated. Therefore, we conclude that Thy-1 binding to $\alpha_v\beta_3$ integrin in cis is via Thy-1's RLD integrin-binding motif, and this interaction appears facilitated by the GPI anchor of Thy-1.

Thy-$1^{D37E}$-expressing fibroblasts were additionally unable to recruit Fyn to the FA, and force- and Thy-1–dependent SFK activation was significantly abrogated (Fig. 4 e). Enhanced force-dependent RhoA activation mediated by Thy-1 was also not supported by Thy-$1^{D37E}$ (Fig. 4 f), demonstrating this motif is critical in Thy-1–dependent mechanosignaling. Cortical stiffening, cell spreading, and FA sensitivity to substrate rigidity were also not conferred by Thy-$1^{D37E}$ (Fig. 4, g–i). Together, these data demonstrate that Thy-1's cis integrin-binding activity is critical for the function of Thy-1 in conferring efficient, physiological mechanosensitivity through the recruitment of Fyn to FN-mediated adhesion complexes.

### Integrin avidity to FN is decreased by Thy-1 cis binding and alters soft ECM sensing

If Thy-1 binds to inactive $\alpha_v\beta_3$ in cis, we hypothesized that in addition to its role in tethering integrin to membrane rafts, Thy-1 engagement of integrin may partially compete with binding to ECM ligands. To investigate this, we used single-cell force spectroscopy to measure the kinetics of integrin binding and avidity during initial (i.e., <5 s) contact with ligand (Fig. 5, a and b). Absence of Thy-1 (empty vector control RFL-6s) resulted in a significantly enhanced binding rate (more than two-fold decreased rate constant, $K$) to FN (Fig. 5, c and d). Early avidity differences observed within the first 2 s of contact were largely normalized as contact time lengthened; Thy-$1^{WT}$ adhesion became comparable to empty vector control cells. Mutation of the RLD motif in Thy-1 (Thy-$1^{D37E}$) also resulted in enhanced avidity to FN, suggesting that the cis integrin-binding function of Thy-1 was indeed responsible for reducing the adhesion rate of integrin to FN (Fig. 5, b and c). Importantly, these Thy-1–dependent differences in adhesion rate were normalized in the presence of cyclic RGD peptide at a concentration that preferentially blocks $\alpha_v\beta_3$-FN interactions (Pierschbacher and Ruoslahti, 1987), suggesting that RGD-binding integrins, like $\alpha_v\beta_3$, are responsible for Thy-1–dependent differences in adhesion to FN (Fig. S4, a and b). These data altogether suggest that in addition to Thy-1 playing an adaptive role in controlling SFK localization and activity, it also modulates integrin activity by functionally "competing" with its ECM ligand.

Cell spreading on ECM-coated rigid substrates has been extensively used as a model system for determining molecular mechanisms involved in mechanosensing (Wolfenson et al., 2014). During initial cell contact, integrin binding and clustering (so-called P0 phase) is required for subsequent rapid and isotropic cell spreading (P1 phase; Dubin-Thaler et al., 2004; Wolfenson et al., 2014). Consistent with a role for Thy-1 in initial integrin binding, immunostaining for active $\alpha_v\beta_3$ integrin demonstrated enhanced integrin activation throughout the cell periphery during initial contact of Thy-$1^{neg}$ RFL-6s (empty vector control) with FN-gl (Fig. 5, e and f). This enhanced integrin activation also correlated with enhanced SFK activity within the cell periphery. Intriguingly, investigation of cell-level spreading dynamics showed that whereas Thy-$1^{WT}$–expressing cells displayed the typical lag phase in spread area associated with integrin binding and clustering, empty vector control RFL-6s did not display an apparent lag phase (i.e., shorter P0) but instead exhibited a more gradual increase in cell area throughout the spreading process (Fig. S4, c and d). In the final stages of cell spreading where fibroblasts undergo successive rounds of protrusion and retraction, during which substrate rigidity is effectively sensed and FAs mature on rigid substrates (Gi-
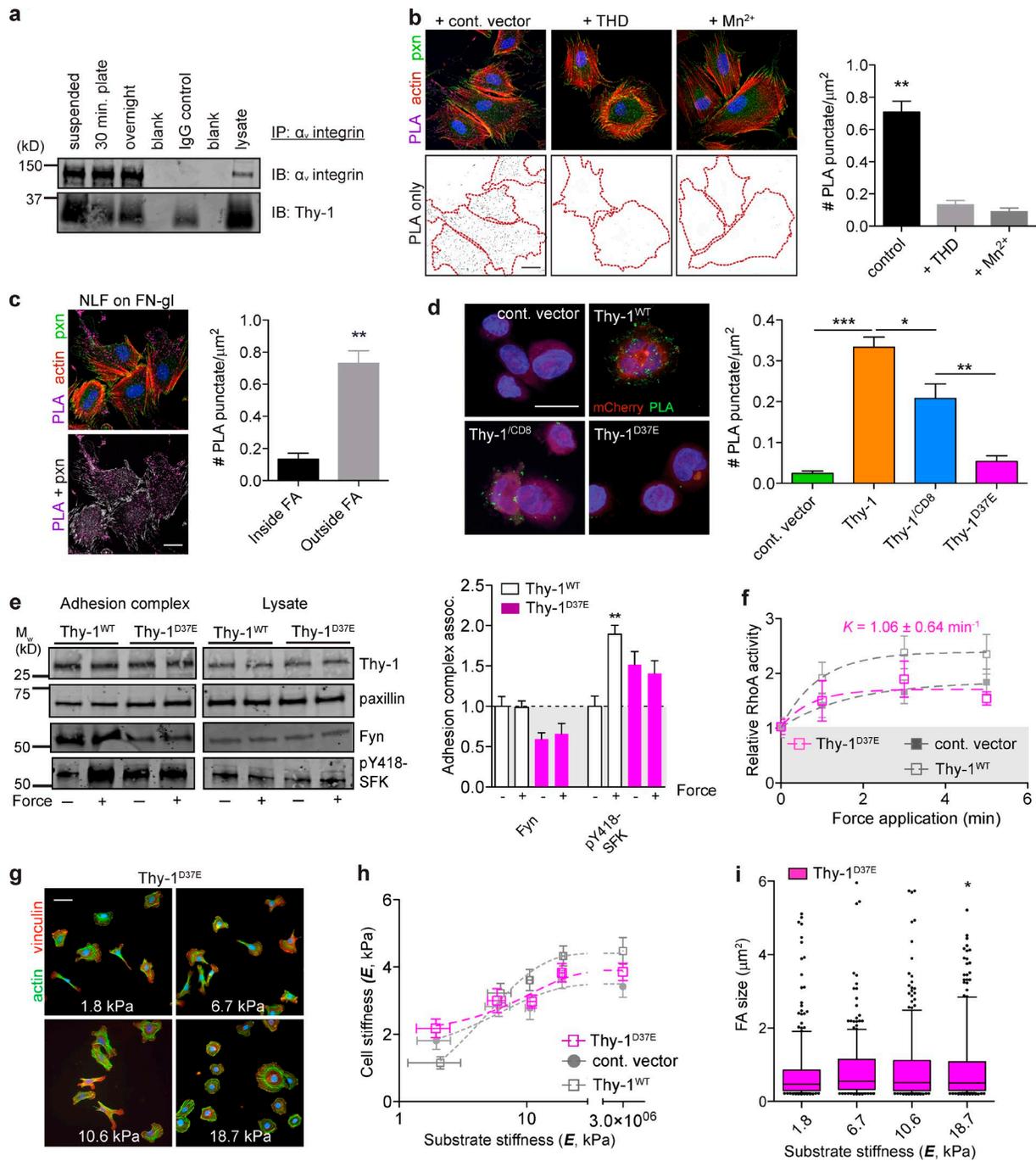
Figure 4.  **Thy-1 binds inactive $\alpha_v\beta_3$ and is required for membrane raft recruitment to FAs, mechanosignaling, and rigidity sensing.** (a) $\alpha_v$ integrin was immunoprecipitated from human NLFs in suspension versus spread on FN for 30 min or overnight, and $\alpha_v$ and Thy-1 were immunoblotted. (b) Micrographs of PLA between $\alpha_v\beta_3$ (mAb 23C6) and Thy-1, pxn immunostaining, and F-actin in NLFs treated with nonbinding control talin (1–405)$^{A/E}$ (cont. vector), wild-type THD (1–405), or 2 mM $Mn^{2+}$ integrin activating conditions. Quantification of PLA cell surface density (mean ± SEM). Bar, 20 µm. (c) PLA signals were masked with pxn immunostaining and the surface density of PLA was segregated into inside versus outside FAs regions and quantified. Bar, 20 µm. (d) Quantification of PLA cell surface density in CHO.B2(h$\alpha_v\beta_3$) expressing human Thy-1$^{WT}$, Thy-1$^{/CD8}$, and Thy-1$^{D37E}$. PLA puncta, mCherry (transfection control), and cell nuclei are shown. Bar, 20 µm. (e) Immunoblots of proteins associated with adhesion complex or total lysate before (− force) or after (+ force) 3 min force application in Thy-1$^{WT}$ and Thy-1$^{D37E}$ RFL-6 cells. Averages of $n = 3$ independent experiments for association with FN-bead adhesion complexes before (− force) or after 3 min force application (+ force) were quantified. Significance was calculated between all groups for individual adhesion components. (f) Activation of RhoA after magnetic force stimulation of FN beads for the indicated time periods in Thy-1$^{D37E}$ RFL-6 cells. Apparent rate constant ($K$) for a single-phase association model is indicated; plateau phase of Thy-1$^{D37E}$ was statistically different from Thy-1$^{WT}$ ($n = 5$; unpaired $t$ test, P < 0.05). Immunostaining for FAs and F-actin (g), single-cell cortical stiffness measurements (h), and FA size (i) of Thy-1$^{D37E}$ RFL-6 cells on FN-PA substrates of varying stiffness. Bar, 50 µm. Statistical significance was calculated using Kruskal-Wallis nonparametric test with Dunn's multiple comparison. All other statistical significance was calculated using one-way analysis of variance and Tukey's post test. *, P < 0.05; **, P < 0.01; ***, P < 0.001 between indicated groups.
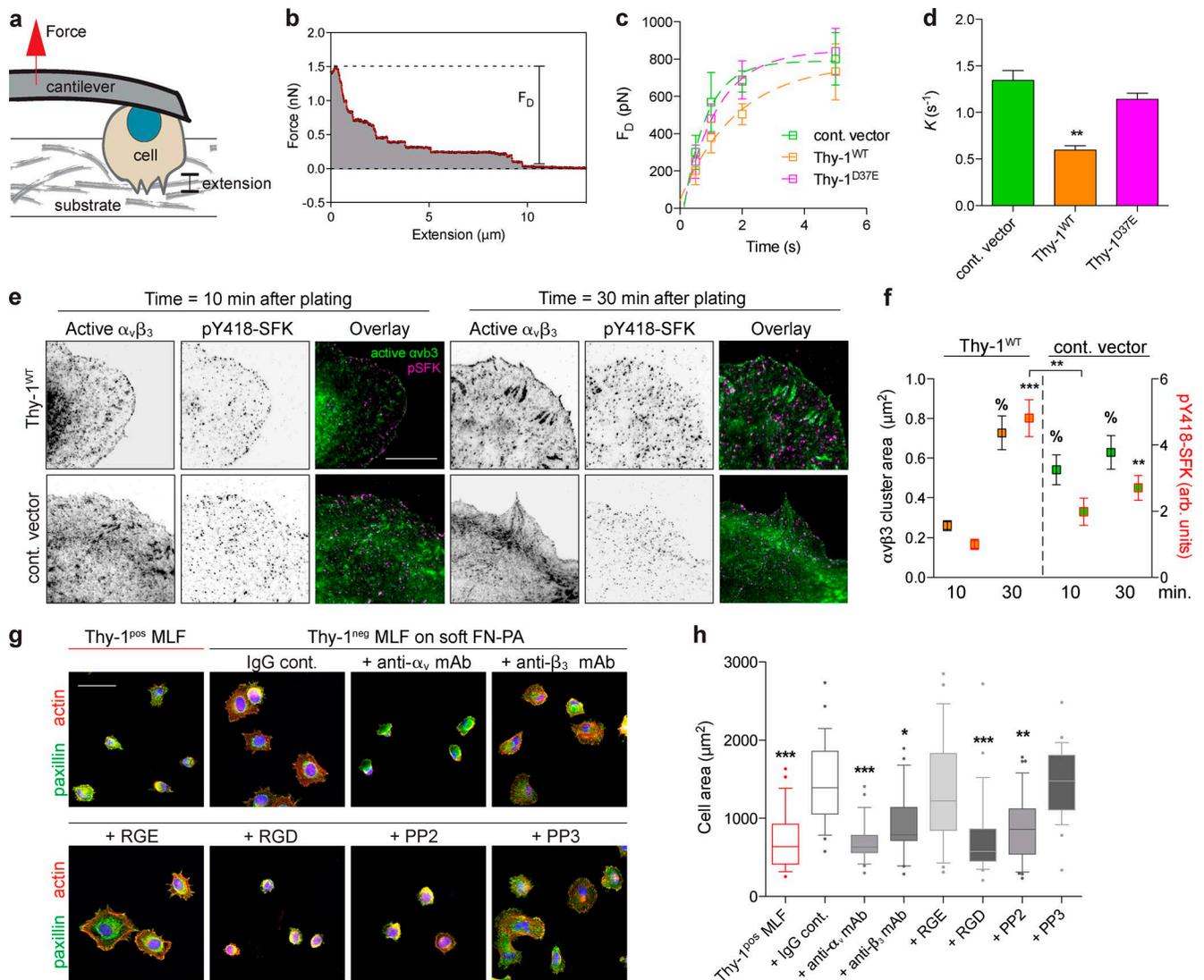
Figure 5. **Integrin avidity to FN is decreased by Thy-1 cis binding and modulates SFK-mediated soft ECM sensing.** (a) Schematic of the single-cell force spectroscopy assay. Cells are attached to an AFM cantilever via physioadsorption of concanavalin A and then touched to a ligand-coated substrate (FN-gl) with controlled force and contact duration. The probe is then extended from the substrate, and the resultant detachment forces are measured. (b) An example force versus extension curve is shown. Individual unbinding events are observed as steps in the force trace, and the maximum detachment force, $F_D$, is indicated. Smoothed data using the Savitsky-Golay method are shown in red. (c) $F_D$ was measured for varying contact times in RFL-6 cells expressing Thy-1$^{WT}$, Thy-1$^{D37E}$, or control vector constructs. $F_D$ versus contact time curves for ~50 contacts in three to five individual cells were fit with a single-phase association model. Data shown are mean ± SD pooled from two independent experiments. (d) Adhesion rate (apparent rate constant, $K$) decreases because of Thy-1$^{WT}$, but not in the RLD mutant. (e) RFL-6s were plated on 10 µg/ml FN-gl, fixed after 10 or 30 min, and stained for active $\alpha_v\beta_3$ (WOW-1) and active SFK (pY418-SFK) to measure integrin clustering and activity during initial cell spreading. Bar, 20 µm. (f) Integrin cluster size (black, left) and pY418-SFK (red, right) were quantified (see Materials and methods). Statistical marks (percentage for $\alpha_v\beta_3$ cluster size; $P < 0.001$) indicate significance with respect to Thy-1$^{WT}$ at 10 min except where indicated. (g) Blocking integrin binding or SFK signaling normalizes aberrant mechanotransduction effects of Thy-1 loss on soft ECMs. Cell spreading of Thy-1$^{pos}$ (red) or Thy-1$^{neg}$ MLFs on soft (1.8 kPa) FN-PA treated with 10 µg/ml IgG control or function-blocking anti-$\alpha_v$ or anti-$\beta_3$ antibodies, RGD or negative control RGE (0.5 mM), and SFK inhibitor PP2 or its negative control PP3 (10 µM) is shown. Bar, 50 µm. (h) Cell area was quantified and represented as box-and-whisker plots (10th–90th percentiles with outlier points shown). Significance with respect to IgG-treated Thy-1$^{neg}$ MLFs is shown. All statistical significance was calculated using one-way analysis of variance and Tukey's post test. *, $P < 0.05$; **, $P < 0.01$; ***, $P < 0.001$ between indicated groups.

annone et al., 2004), this transition was more pronounced because of Thy-1$^{WT}$ expression, coincident with FA enlargement (Fig. S4, c and d). During this time period, Thy-1$^{WT}$–expressing cells also exhibited more active SFK, which we speculate is due to enhanced force-dependent Fyn activation, as has been previously implicated in adhesion reinforcement and rigidity sensing (von Wichert et al., 2003; Kostic and Sheetz, 2006; Guilluy et al., 2011). These patterns of SFK activity during the largely force-independent P1 phase of cell spreading and the

force-dependent P2 phase strongly correlate with our data from magnetic force-pulling assays (Fig. 2).

We were interested in whether enhanced integrin avidity and SFK signaling at early time points in the absence of Thy-1 results in the altered mechanosensing of soft matrix observed in Thy-1$^{neg}$ cells (Fig. 5, g and h). When Thy-1$^{neg}$ MLFs cultured on soft FN-PA substrates were treated with soluble RGD, their spread area and FA size were dramatically reduced, normalizing their response to that of Thy-1$^{pos}$ fibroblasts.

Function-blocking antibodies further confirmed the $\alpha_v$ integrin dependency of these responses. In a similar fashion, pan-specific blockade of SFKs using the pharmacological inhibitor PP2 resulted in a similar reduction of cytoskeletal activity. Thus, we can conclude that the aberrant rigidity sensing of soft ECMs in Thy-1^{neg} fibroblasts can be abrogated by inhibiting the elevated integrin ($\alpha_v$)/SFK activity seen in these cells during low-force/soft-matrix conditions.

### Thy-1 loss dysregulates rigidity-dependent ECM assembly and fibroblast activation

To assess the potential pathophysiological consequences of altered rigidity sensing in the IPF-associated fibroblast subpopulations, we analyzed phenotypes of fibroblast isolates from IPF patients. IPF LFs were sorted into subpopulations of Thy-1^{neg} (5–15% of initial population) or Thy-1^{pos} IPF LFs, whereas normal lung fibroblasts (NLFs) were a single population (>95% Thy-1^{pos}; Fig. S5). One of the hallmarks of fibrotic progression is fibroblast-to-myofibroblast differentiation, characterized by enhanced ECM synthesis and assembly and increased resistance to apoptosis. Analysis of type I procollagen expression and FN fibrillogenesis (a cytoskeletally driven process) via immunofluorescence staining (Fig. 6 a) and deoxycholate (DOC) insolubility (Fig. S5 e) demonstrated activation of ECM assembly in Thy-1^{neg} IPF LFs, but not NLFs or Thy-1^{pos} IPF LFs, on soft substrates. Thy-1^{neg} IPF LFs also display significant proliferation and resistance to apoptosis on soft substrates (Fig. 6, b and c). As expected, stiff substrates induce myofibroblastic phenotypes in NLFs and both IPF LF subpopulations. Together, these data are indicative of myofibroblastic differentiation of Thy-1^{neg}, but not normal or Thy-1^{pos}, IPF LFs on soft substrates, suggesting a role for Thy-1 in dysregulated myofibroblast differentiation. To further verify a specific role for Thy-1, we performed shRNA knockdown experiments. Control NLFs (control shRNA) exhibited cytoskeletal phenotypes (i.e., cell spreading, cortical stiffness, and FA size; Fig. 6, d–f) consistent with Thy-1–expressing MLFs and RFL-6 cells (Fig. 1), whereas Thy-1 knockdown (Thy-1 shRNA; 90% knockdown efficiency; Fig. S5 c) increased contractility on soft substrates. Furthermore, Thy-1 knockdown enabled highly efficient FN assembly on soft ECMs that resemble the stiffness-induced phenotypes observed in NLFs (Fig. 6 g). This is also consistent with the effect of elevated integrin activation promoting FN assembly on soft substrates (Carraher and Schwarzbauer, 2013). Furthermore, control shRNA NLFs (i.e., Thy-1^{pos}) exhibited RhoA activity levels (Fig. 6 f) that robustly and predictably correlated with substrate stiffness, whereas Thy-1 knockdown induced enhanced and rigidity-insensitive RhoA activity. Addition of Rho kinase inhibitor Y-27632 eliminated Thy-1–dependent effects on cell spreading (Fig. 6 f). As a final confirmation of physiologically relevant cytoskeletal activation, we tested the ability of Thy-1 knockdown to promote fibroblast contraction in soft ($E = 300$ Pa) 3D collagen gels. As expected, Thy-1^{neg} fibroblasts contracted soft FN-containing collagen matrices more efficiently than did Thy-1^{pos} (Fig. 5 h), a response mediated by Rho kinase. These data strongly suggest a significantly enhanced profibrotic phenotype of Thy-1^{neg} fibroblasts in soft, physiological ECMs that are representative of normal lung and that aberrant mechanosensitivity, because of the loss of Thy-1 surface expression, can result in fibroblast activation in normally nonpermissive microenvironments.

## Discussion

In this work, we identify a unique complex formed between the GPI-anchored cell-surface protein Thy-1 and $\alpha_v\beta_3$ integrin that appears to function upstream of canonical ECM-integrin ligation and FA formation. The proximity of Thy-1 and its RGD-like integrin-binding motif to the plasma membrane ($\sim$2–5 nm) likely requires that integrin be in its inactive, bent versus "active" conformation (i.e., ligand-binding head domains extended $\sim$20 nm from the membrane surface) to facilitate binding, implying the interaction occurs preferentially outside of FAs and before (i.e., upstream) integrin engagement of extracellular ligands. Our Thy-1–$\alpha_v\beta_3$ PLA localization data using conformation-specific integrin antibodies support this hypothesis. Furthermore, the requirement of Thy-1–integrin–membrane raft tripartite interactions in mediating Fyn recruitment to FAs, force-dependent RhoA activation, and fibroblast rigidity sensing underscores the functional importance of this upstream complex. Intriguingly, multiple membrane raft–associated outer membrane proteins (e.g., uPAR, GPI-80, and CD47) have been shown to associate with integrins in cis and alter their signaling function (Wei et al., 1996, 2005; Brown and Frazier, 2001; Yoshitake et al., 2003). A question arising from our work, in light of these other studies, is whether these structurally similar proteins constitute a functional family of upstream integrin adaptors that modulate FA signaling. We hypothesize that the role for such adaptors is to spatially couple inactive signaling molecules to inactive integrin receptors in preassembled (i.e., "primed") clusters, such that downstream signals are generated and propagated rapidly upon ligand binding or application of forces—a so-called preadhesion complex (Fig. 7). In support of this theory, previous work has shown that cross-linking of multiple nanoscopic clusters of Thy-1 and other GPI-anchored proteins is sufficient to activate SFKs and cause local actin remodeling on the millisecond timescale (Chen et al., 2006). Furthermore, and in support of our data demonstrating Thy-1–mediated recruitment of Cbp to FAs, cytoskeletal engagement of antibody-induced Thy-1 clusters was previously shown to be dependent on Cbp (Chen et al., 2009). However, direct testing of the molecular dynamics of this mechanism should be the focus of future investigation.

It has been long demonstrated that membrane rafts play a critical role in integrin signaling at FAs, as many adhesion-associated signaling molecules such as Fyn, FAK, and Rac1 associate with detergent-resistant membrane fractions (Shima et al., 2003; del Pozo et al., 2004; Palazzo et al., 2004). FAs have a higher level of liquid-ordered membrane than do surrounding regions of the plasma membrane (Gaus et al., 2006), and localization of specific membrane raft components (e.g., Rac1) is modulated by integrin engagement (del Pozo et al., 2004; Norambuena and Schwartz, 2011). Intriguingly, the majority of integrins in the nonligated state are found in nonraft fractions (Leitinger and Hogg, 2002). However, it was recently demonstrated that inactive integrins exist in nanodomains that are spatially separate from but immediately adjacent to nanodomains of GPI-anchored proteins, and these domains coalesce upon integrin binding (van Zanten et al., 2009). Therefore, it appears that under basal conditions, integrins have some affinity toward nanodomains of GPI-anchored proteins; however, the origins of this affinity are not fully understood. By virtue of its ability to bind latent integrin and localize to membrane rafts, we suggest that Thy-1 represents a plausible integrin-raft coupling adapter
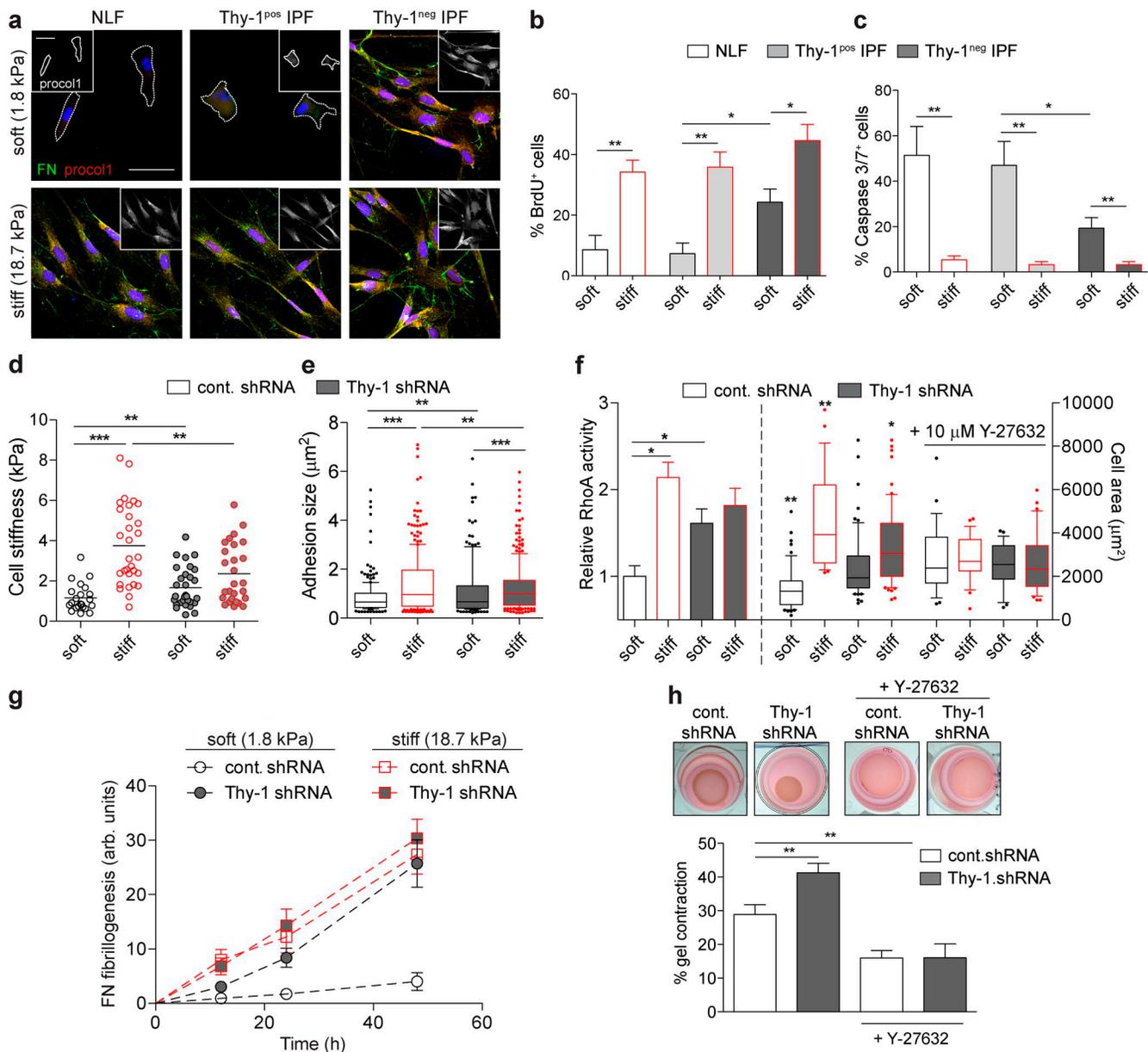
Figure 6. **Thy-1 loss dysregulates rigidity-dependent ECM assembly and fibroblast activation.** (a) Immunofluorescence of FN and procol1 (also inset) in human NLFs and Thy-1$^{pos}$ and Thy-1$^{neg}$ IPF LFs cultured on soft (1.8 kPa) versus stiff (18.7 kPa) FN-PA for 48 h. Cell periphery is denoted in cells with low expression of FN/procol1 only. Bar, 50 μm. Quantification of BrdU incorporation (b) and Caspase3/7 staining (c) for primary human LFs cultured on soft (black outline) and stiff (red outline) FN-PA substrates for 4 d. (d) Single-cell stiffness was measured for control shRNA (white) and Thy-1 shRNA (gray) NLFs cultured on soft (black outline) and stiff (red outline) FN-PA substrates. (e) Box-and-whisker plots (10th–90th percentiles with outlier points shown) of FA area for a minimum of $n$ = 10 cells are shown. Statistical significance was calculated using Kruskal-Wallis nonparametric test with Dunn's multiple comparison. (f) RhoA activity (left) and cell area (right) of control shRNA- or Thy-1 shRNA-treated NLFs on soft (black outline) and stiff (red outline) FN-PA gels. For cell area quantification, cells were treated with or without 10 μM Y-27632. (g) Quantification of cell-associated FN assembly (mean ± SEM; area × intensity, arbitrary units) for control shRNA and Thy-1 shRNA NLFs on soft versus and stiff FN-PA substrates over time. (h) Images of 1.7 mg/ml collagen I gels contracted by fibroblasts after 48 h in culture. Gel contraction was quantified (percentage of the original gel diameter) for control shRNA and Thy-1 shRNA NLFs with and without 10 μM Y-27632 treatment. All statistical significance was calculated using one-way analysis of variance and Tukey's post test except where otherwise stated. *, $P < 0.05$; **, $P < 0.01$; ***, $P < 0.001$ between indicated groups.

protein. Intriguingly, complex formation between the GPI anchor mutant Thy-1 (Thy-1$^{/CD8}$) and $\alpha_v\beta_3$ was not as efficient as Thy-1$^{WT}$ despite the presence of the wild-type RLD motif. We offer two plausible explanations for these data. First, features of the local plasma membrane environment, determined in part by Thy-1's endogenous GPI targeting, could facilitate the efficient coupling of Thy-1 and $\alpha_v\beta_3$. Alternatively, changes in Thy-1's conformation caused by GPI anchor substitution may decrease

the affinity of Thy-1 to integrin, as Thy-1's GPI anchor is known to affect its conformation (Barboni et al., 1995).

Thy-1 coupling with integrin appears to modulate FA mechanosignaling via multiple mechanisms. Although cis interactions with Thy-1 enable recruitment of critical membrane raft components to FAs, this interaction also diminishes baseline integrin avidity to ECM ligands and early SFK signaling during initial substrate contact. Although the exact structural dynamics of the
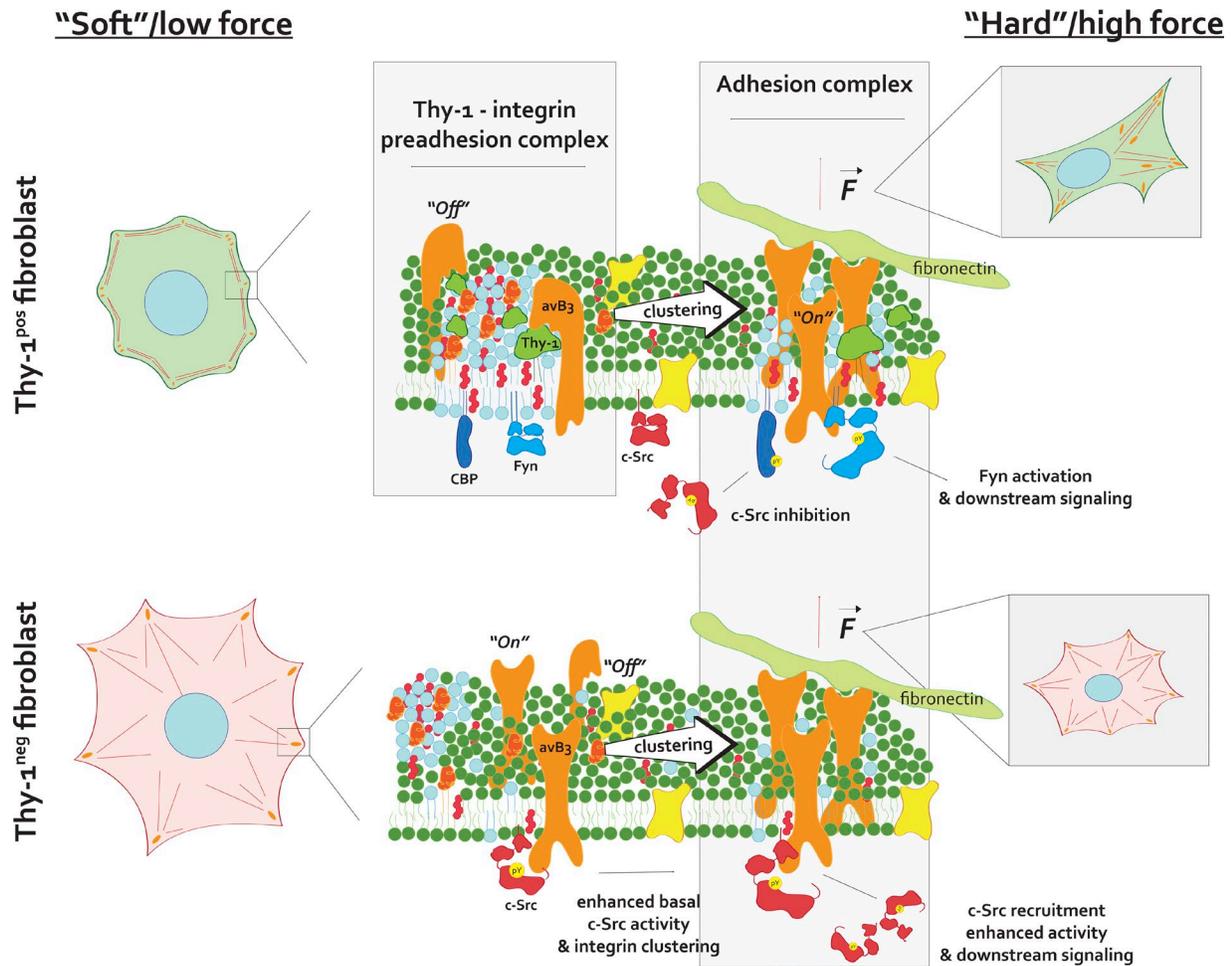
**Figure 7.  A mechanistic model of Thy-1's effects on integrin avidity and signaling.** Thy-1 binds $\alpha_v$ integrins preferentially in their inactive, "off" state, which couples integrins with membrane raft domains and their localized signaling molecules, such as Fyn and Cbp, before FN recognition (top, left). FN binding and receptor clustering enriches for these domains within growing FAs while promoting conformation-dependent integrin/SFK accessibility of binding motifs and sensitive responses to stimuli (e.g., force; top, right). In the absence of Thy-1, a higher probability of $\alpha_v$ integrin binding to FN exists, thus eliciting elevated levels of baseline integrin signaling, potentially through c-Src recruitment and activation (bottom, left). As a result of decoupling of integrin and membrane rafts, raft-associated molecules (Fyn, Cbp) are no longer recruited to growing FAs and sensitive signaling (e.g., Cbp-dependent negative feedback on c-Src regulation and force-dependent Fyn activation) is not as prominent (bottom, right).

proteins within the Thy-1–$\alpha_v$ complex cannot be inferred from our data, we propose that (a) Thy-1 partially competes with integrin binding to ECM ligands, altering the energy landscape of initial integrin binding, and (b) concurrently acts to couple integrin to raft domains, facilitating recruitment of raft-associated signaling molecules to nascent FAs (Fig. 7). It is known that both integrins and SFKs exist in a series of conformations related to their activation state. Interactions between the SH3 domain and flexible linker region stabilize inactive SFKs in a clamped and sterically inaccessible state (Brown and Cooper, 1996; Thomas and Brugge, 1997). Binding of the SH3 domain to associating adapters relieves the autoinhibitory conformation, thus priming the molecule for further activation (Brown and Cooper, 1996; Shattil, 2005). In the case of c-Src and $\beta_3$ integrin, this autoinhibition is relieved by SH3 domain binding to the C-terminal Arg-Gly-Thr motif, which is sufficient for subsequent integrin-clustering–mediated trans-autoactivation of c-Src and downstream signaling (Arias-Salgado et al., 2003, 2005). Consistent with a critical role for c-Src in early FA signaling, c-Src phosphorylates FHOD1 in response to integrin clustering (Iskratsch et al., 2013) and p190GAP to inactivate RhoA and drive actin polymerization during cell spreading (Arthur et al., 2000;

Arthur and Burridge, 2001). The fact that these responses (integrin avidity, early cell spreading, and local SFK activity) are elevated in the absence of Thy-1 supports that c-Src interaction with integrin is direct and that the loss of Thy-1, which skews nonligated integrin toward its active/avid state, enables rapid clustering-dependent elevated c-Src signaling. Intriguingly, unlike c-Src, a specific binding motif for the raft-associated Fyn is within the membrane-proximal HDRK motif in the $\beta_3$ subunit, which is also the site for $\alpha/\beta$ integrin intersubunit salt bridge formation (Reddy et al., 2008; Legate and Fässler, 2009). This suggests that in the bent and membrane-proximal clasp-stabilized integrin, Fyn cannot access its SH3 binding site, thus inhibiting direct association with integrin. Thereby, Thy-1 may enable coupling of inactive (i.e., clamped) Fyn molecules in close proximity to low-affinity integrin molecules (i.e., bent conformation), supporting temporally efficient signal transduction (i.e., SFK priming and activation) in response to integrin ligation, clustering, and/or mechanical forces while simultaneously facilitating the use of SFK's multiple regulatory mechanisms. Temporally efficient mechanoactivation of RhoA, which is critically dependent on Thy-1 and regulated by Fyn, further supports this hypothesis.

A major theory in fibrosis posits that the mechanical microenvironment, specifically tissue stiffness, drives transformation of stromal cells to highly active myofibroblasts, which further remodel the tissue leading to disease progression (Tomasek et al., 2002; Georges et al., 2007; Liu et al., 2010; Huang et al., 2012). The work presented here provides an interesting new perspective on the dynamic reciprocity between fibroblast phenotypes and microenvironment cues implicated in the initiation of progressive fibrosis. Our data suggest that the investigation of activated cell phenotypes within microenvironments representing normal, wound healing, or new/ongoing fibrosis (i.e., soft environments), rather than mature or established fibrosis (i.e., stiff environments), may be essential to understanding disease initiation. It is worth noting that mechanosensitivity of carcinoma-associated fibroblasts (CAFs) plays a critical role in potentiating cancer progression through assembly and remodeling of the tumor stroma (Calvo et al., 2013). As peritumoral CAFs are typically marked by high Thy-1 expression (True et al., 2010; Goetz et al., 2011; Samaniego et al., 2013), this suggests that deleterious phenotypes (i.e., mechanosensitive CAF responses to solid tissue stress during tumorigenesis versus decreased mechanosensitivity in Thy-1^{neg} IPF fibroblasts during fibroblastic foci formation) depend critically on the microenvironmental context and disease course. Understanding how changes in fibroblast phenotype and possible dysregulated signaling within a dynamic ECM results in matrix remodeling and eventual stiffening of the microenvironment driving disease progression is a rich area for future research.

## Materials and methods

### Cell culture and plasmids

Primary MLFs were isolated from 6- to 8-wk-old C57/Bl6 mice (McIntosh et al., 1994). Mouse lungs were lavaged with sterile PBS, the pulmonary vasculature was perfused with heparin-supplemented PBS, and then lungs were excised. After dissection of lobes 1–5, lung parenchyma was minced and subject to enzymatic disruption (0.4 mg/ml DNaseI, 1 mg/ml collagenase, and 0.05% trypsin; Sigma-Aldrich) and plated onto tissue culture polystyrene. Medium was changed every 48 h, and cells were subcultured at 1:3. Cells were maintained in DMEM supplemented with 10% FBS, 100 µg/ml penicillin/streptomycin, and 1 mM sodium pyruvate (normal growth medium). Early-passage MLFs (P3–P5) and c-Src/Yes/Fyn-knockout MEFs (Klinghoffer et al., 1999; SYFs; ATCC) were sorted for Thy-1 expression using FACS (FACSAria III; BD) after staining with FITC-labeled anti–CD90.2 monoclonal antibody (1:200, 53-2.1; BD). Cells were subcultured and resorted in normal growth medium until subpopulations of >90% purity were obtained. SYFs were transfected with 1 µg EGFP-tagged c-Src or Fyn under the immediate early cytomegalovirus promoter in EGFP-N1 vector (a gift from M. Frame, Edinburgh Cancer Research Center, Scotland, UK; Sandilands et al., 2007) using an Amaxa Nucleofector kit T (Lonza) and program U-30. 24 h later, cells were plated on PA substrates of varying stiffness and analyzed for cell spread area as described below. CHO.B2 cells (a gift from M. Humphries, University of Manchester, England, UK) were cultured in DMEM + 10% FBS, 100 µg/ml penicillin/streptomycin, and 1× MEM nonessential amino acids (Gibco). To obtain the CHO.B2($h\alpha_v\beta_3$) line, CHO.B2 cells were stably transfected with human $\alpha_v$ subunit isoform 2 in pEF1/V5-HisA vector (plasmid 27290; Addgene) and human $\beta_3$ subunit in pcDNA3.1/Myc-His(+)A vector (plasmid 27289; Addgene) and FACS-isolated for stable expression using mAb 23C6 (Millipore). For PLA experiments,

CHO.B2($h\alpha_v\beta_3$) were transiently transfected with 1 µg human Thy-1 constructs (detailed below) and mCherry in pmCherry-N1 vector (transfection control) using Amaxa Nucleofector kit T (Lonza) and program U-23. Cells were allowed to recover overnight and then plated on FN-gl and allowed to spread for 4 h before fixation and staining. RFL-6 cell lines were made to stably express mouse Thy-1.2 constructs under the constitutive cytomegalovirus promoter. The 480-bp mouse *Thy-1.2* cDNA containing the full-length coding sequence was isolated from a pBluescript SK+ plasmid by digestion with EcoRI and XhoI, purified by gel electrophoresis, and ligated into the mammalian expression system pcDNA3.1Zeo+ (Invitrogen) at the EcoRI and XhoI sites. Constructs were sequenced for verification. Embryonic rat LFs (RFL-6) were transfected with either the empty pcDNA3.1Zeo+ expression vector (empty vector control) or the expression vector containing mouse Thy-1 cDNA (Thy-1[WT]) using the transfection reagent LT-1 (Mirus), and stable clones were selected by culture in the presence of 100 µg/ml Zeocin (Invitrogen). Flow cytometry analysis was performed (FITC–Thy-1.2, 53-2.1; BD) using an Accuri C6 (BD) to verify populations containing >90% Thy-1^{pos} fibroblasts expressing Thy-1 at levels similar to those of wild-type Thy-1^{pos} fibroblasts for experimentation. Cells were maintained and subcultured in Ham's F12 (CellGro) supplemented with 10% FBS and 100 µg/ml penicillin/streptomycin.

Primary human LFs were isolated from normal or IPF patients (White et al., 2003). NLFs were obtained from patients undergoing thoracic surgery for nonfibrotic lung diseases. IPF LFs were used from patients in whom a pathological diagnosis of UIP was subsequently made. Written informed consent was obtained from all subjects in accordance with the University of Michigan Institutional Review Board. Under sterile conditions, lung tissue segments were minced to a fine slurry and plated in T-75 tissue culture flasks in normal growth medium. Media were aspirated and replaced with fresh media every 48–72 h. Cells were passaged using 0.25% trypsin-EDTA and subcultured at 1:3. This resulted in a population of cells with fibroblast morphology that are CD14^{neg}, pan-keratin^{neg}, vimentin^{pos}, and factor VIII^{neg}. For FACS, cells were stained with FITC-labeled anti–human Thy-1 antibody (1:200, 5E10; BD) and sorted into Thy-1^{pos} and Thy-1^{neg} subpopulations based on equivalent positive expression of NLFs or negative antibody controls, respectively. Cells were used for experimentation between passages 4 and 9 (P4–P9). For Thy-1 knockdown experiments, CCL-210 NLFs (ATCC) were transduced with lentiviral particles (5× MOI plus 5 µg/ml Polybrene) containing a pool of target-specific constructs (sc-32837-v; Santa Cruz Biotechnology) or a scrambled sequence control without specificity to any known cellular mRNA (sc-108080). Hairpin sequences are as follows: 5′-GATCCTCAGAGACAAACTGGTCAATTCA AGAGATTGACCAGTTTGTCTCTGATTTTTT-3′ (sc-42837-SHA), 5′-GATCCGTGCAGAGATCCTACTTCTTTCAAGAGAAGAAG TAGGATCTCTGCACTTTTT-3′ (sc-42837-SHB), 5′-GATCCTGC TGCATGCGATTATCTATTCAAGAGATAGATAATCGCATGCAGCAT TTTT-3′ (sc-42837-SHC). After 72 h, transduced cells were subcultured and selected with 1.0 µg/ml puromycin. Cells were sorted by FACS for knockdown efficiency, whereas the control shRNA construct had no effect on Thy-1 expression. For RNAi rescue experiments, Thy-1 shRNA NLFs were transfected with 1.0 µg mouse Thy-1[WT] or Thy-1[D37E] constructs using Nucleofector program U-023 and plated on FN-PA substrates 24 h later for cell spreading or flow cytometry analysis.

Wild-type human or mouse Thy-1 (Thy-1[WT]) in pcDNA3.1Zeo+ (Bradley et al., 2013; Invitrogen) was used to substitute aspartate aa37 to glutamate (Thy-1[D37E]). Primers (Integrated DNA Technologies) used for site-directed mutagenesis were 5′-ACCAGAGCCTTCGTCTGG AGTGCCGCCATGAGAATACC-3′ and 5′-GGTATTCTCATGG CGGCACTCCAGACGAAGGCTCTGGT-3′. For Thy-1 GPI-anchor mutations, the C-terminal cysteine (aa130) of the mature glycoprotein

was connected via a short linker (GGIGLS) to the CD8 transmembrane sequence (DIYIWAPLAGICVALLLSLIITLICYHSR), as has been previously done (Tiveron et al., 1994). For construction, the following overlapping oligonucleotides were assembled by PCR to generate the CD8 transmembrane sequence: 5′-GTCAAGTGTGGGGGCATC GGCCTGTCCGATATCTATATCTGGGCACCCTTG-3′, 5′-AGGACAGC AGAAGGGCCACGCAGATTCCGGCCAAGGGTGCCCAGATATAGA-TAT-3′, 5′-GGCCCTTCTGCTGTCCTTGATCATCACTCTCATCTGCT ACCACAGCCGCTAATA-3′, 5′-GTTTCTTCCTGCAGCGGCCGCTA CTAGTATTATTAGCGGCTGTGGTAGC-3′, which was subsequently assembled using overlap extension PCR cloning into the parental Thy-1[WT] vector (Bryksin and Matsumura, 2010). Constructs for altering integrin activation were talin1(1–405)-GFP and talin1(1–405)A360E-GFP with integrin-binding–defective mutation (from D. Calderwood, Yale University, New Haven, CT). These constructs consist of residues 1–405 of NP_006280.2, including the entire talin1 FERM domain (F1F2F3) and F0 in the pcDNA3 vector, and the point mutant A360E within F3, which inhibits its binding and activation of $\beta_1$ and $\beta_3$ integrins (Bouaouina et al., 2008).

## Hydrogel substrate preparation

FN-PA hydrogels with varying bisacrylamide concentrations were fabricated on amino-silanized coverslips, as previously described (Brown et al., 2013). In brief, PA gel solutions were produced by combining acrylamide and bisacrylamide (Bio-Rad) to final concentrations of 8% acrylamide and 0.045%, 0.102%, 0.146%, or 0.239% bisacrylamide to obtain gels with final elastic moduli of 1.8 kPa, 6.7 kPa, 10.6 kPa, or 18.7 kPa, respectively. 35 µl of each solution was polymerized by the addition of 1% (vol/vol) ammonium persulfate (VWR) and 0.1% (vol/vol) $N,N,N',N'$-tetramethylethylenediamine (Bio-Rad). Human plasma FN was purified from blood plasma and covalently attached to the surface using 0.2 mg/ml UV-activated heterobifunctional cross-linker sulfosuccinimidyl-6-(4′-azido-2′nitrophenyl-amino)hexanoate (Pierce Chemical). After overnight incubation with 20 µg/ml FN, gels were then washed and stored in PBS.

## Atomic force microscopy (AFM) mechanical measurements

An MFP-3D AFM (Asylum Research) integrated with a TiE inverted optical microscope (Nikon Instruments) was used for all AFM experiments. AFM nanoindentation tests were performed under fluid conditions using a 4.74-µm-diameter spherical tipped-silicon nitride cantilever (MSCT-AU; Bruker). Cantilever spring constants were measured before sample analysis using the thermal fluctuation method, with nominal values of 20–50 pN/nm. Force-indentation curves were individually analyzed using a Hertzian model for contact mechanics of spherical tips, from which Young's modulus was obtained. The sample Poisson's ratio was assumed as 0.33, and a power law of 1.5 was used to model tip geometry, as previously described (Brown et al., 2013). AFM measurements were made using a cantilever deflection set point of ∼2 nN and an indentation rate of 22.86 µm/s. For cell and substrate measurements, cells were plated at $2 \times 10^4$ cells/cm$^2$ and measured within 4–6 h of plating in normal growth medium. Single force points taken from three perinuclear regions >300 nm in height were averaged to determine a cell's mean cortical stiffness. Similarly, regions of FN-PA substrate surrounding measured cells were probed.

Single-cell force spectroscopy experiments were conducted in a similar manner to Friedrichs et al. (2010). AFM probes were cleaned with 1 M $H_2SO_4$ for 1 h before plasma cleaning and incubation with 2 mg/ml concanavalin A from *Canavalia ensiformis* (Sigma-Aldrich) overnight at 4°C. Probes were washed and maintained in PBS until use. Acid-washed and plasma-cleaned borosilicate glass was coated overnight with 5 µg/ml plasma-purified human FN and blocked with 2 mg/ml

heat-denatured BSA. After trypsinization and resuspension, cells were maintained $CO_2$-independent Leibovitz's L-15 medium supplemented with 0.5 mg/ml BSA and 100 µg/ml penicillin/streptomycin, as was the AFM chamber during experimentation. Single cells were captured on the AFM cantilever (cantilever spring constant, k ∼30 pN/nm) and repeatedly brought into contact with the FN-coated surface with a 1 nN contact force and approach and retract rate of 5 µm/s. Retraction force curves were analyzed for the maximum detachment force, $F_d$, and for contact times ranging from 0.5 to 5 s. A single-phase association model, $Y = Y_0 + (\text{plateau} - Y_0) \times (1 - \exp[-K*x])$, was used to compute the apparent rate constant, $K$, for adhesion rate.

## Immunostaining and fluorescence microscopy

Samples were fixed using 4% formaldehyde, permeabilized in 0.2% Triton X-100, and blocked with 5% normal goat serum in PBS. Primary antibodies for vinculin (1:200, mouse, V284; Millipore), paxillin (1:200, mouse, 5H11; Millipore), FAK-pY397 (1:150, rabbit, 44-624G; Invitrogen), mouse Thy-1.2 (1:200, rat; 53-2.1; BD), human Thy-1 (1:200, mouse, 5E10; BD), $\alpha_v\beta_3$ (1:50, mouse, WOW-1; a gift from S. Shattil, University of California, San Diego, La Jolla, CA), pY418-SFK (1:100, rabbit, D49G4; Cell Signaling Technology), and FN (1:300, rabbit, AB2024; Millipore) along with Alexa Fluor–labeled secondary antibodies (1:2,000, goat; Invitrogen) were used. Alexa Fluor–conjugated phalloidin (1:40; Invitrogen) was used to stain F-actin. For GM1-marked membrane raft staining, cells were costained with Alexa Fluor 647–labeled CTxB (2 µg/ml; Invitrogen) and paxillin after fixation with 4% formaldehyde/0.2% glutaraldehyde and permeabilization with 0.2% Triton X-100. All samples were mounted in ProlongGold (Invitrogen), except for total internal reflection fluorescence (TIRF) imaging. Images were acquired using 20× (plan-fluor, 0.5 NA) or 60× (apo-TIRF, 1.49 NA oil) objectives with a Nikon TiE epifluorescence microscope (Nikon Instruments), CoolSNAP HQ2 monochromatic CCD camera (Photometrics), and NIS-Elements acquisition software (v3.2; Nikon Instruments), or using a LSM700 confocal microscope (Carl Zeiss) with a variable secondary dichroic, 20× (plan-apochromat, 0.8 NA) or 60× (plan-apochromat, 1.4 NA oil) objectives, and Zen software (Black; Carl Zeiss) for image acquisition. For TIRF microscopy, images were acquired using the Zeiss Elyra system with iXon EM-CCD camera (Andor Technology) and 100× (plan-apochromat, 1.46 NA oil) objective, and imaging was performed in PBS. All imaging was conducted at room temperature.

## Image quantification

An in-house–built MATLAB (MathWorks) program was used to quantify micrographs based on the morphometry and intensity of FA and cellular features. After background subtraction and intensity thresholding, a mask was generated to identify and isolate structures of based on FA signals (e.g., paxillin, vinculin). Masked pixels were converted to binary sequence, and connected pixels were grouped into bins based on size and converted to µm$^2$ units. Identified structures were matched with corresponding pixel values (intensity, spatial coordinate) of alternate channels, and pixel values were grouped and averaged per individual FA. A size discrimination filter of >10 µm$^2$ was used to remove cytoplasmic and perinuclear staining not associated with FAs. For local GM1-marked membrane raft recruitment to FAs, paxillin was used as an FA marker. CTxB signal was masked with the paxillin signal, and FA-localized intensity of CTxB was measured on a per-pixel basis and averaged for individual subcellular FAs. All FA parameters measured for individual cells were pooled for statistical analysis between experimental groups. For pY418-SFK staining, signal was acquired in the basal portion of the cell using TIRF microscopy, and the mean intensity value of the cell periphery (≤10 µm from the cell edge) was quantified

for individual cells. Cell area was quantified using the same intensity-based detection and binarization scheme in MATLAB or using NIS-Elements (v3.2; Nikon Instruments) autothreshold and binarization feature based on phalloidin or DiI staining.

## Magnetic tweezing and adhesion complex precipitation

$2 \times 10^6$ cells/dish were plated in a 10-cm tissue culture–treated polystyrene dish and made quiescent overnight in serum-free DMEM containing 0.5% BSA. 2.8 μm–diameter magnetic beads (M280 Dynabead; Invitrogen) coated with full-length FN or anti–transferrin receptor (CD71, H-300; Santa Cruz Biotechnology) were added at a 10:1 ratio of beads per cell in serum-free DMEM plus 0.5% BSA. After a 15-min period to allow bead binding, a neodymium permanent magnet with (N42 grade, DZ04; K & J Magnets) was placed 6 mm from the dish surface. After the prescribed time of magnetic force application, cells were lysed (10 mM Hepes, pH 7.6, 150 mM NaCl, 0.1% NP-40, and 2 mM $MgCl_2$ plus protease inhibitor cocktail), the bead fraction was precipitated magnetically (DynaMag; Invitrogen) and both the bead and supernatant fractions were collected. The bead fraction was washed with lysis buffer, and coprecipitated proteins were immediately denatured in 2× Laemmli buffer, separated from magnetic beads, and aliquoted for immunoblot analysis. Equal sample volume was loaded for SDS-PAGE, and lysate samples (both whole cell and supernatant) were prepared and analyzed for each experiment to ensure equivalent protein expression and handling between samples. Force levels applied using this setup were between 10 and 16 pN per bead as verified using COMSOL simulations and according to those published previously (Guilluy et al., 2011). For COMSOL simulations, the magnetic field gradient and flux density ($B$) of the 1.32-kG magnet was calculated, and magnetic force ($F_b$) as a function of radius was solved for using the known experimental parameters (axial distance, bead diameter, and permeability constants).

## Immunoprecipitation and Western blots

Cells were maintained in suspension or plated at $5 \times 10^4$/cm$^2$ in a 10-cm diameter dish. Cells were lysed in 50 mM Tris, pH 8.0, 150 mM NaCl, 5 mM EDTA, 5% glycerol, 1% Triton X-100, and 25 mM NaF and supplemented with 1× cOmplete Protease Inhibitor and PhosSTOP phosphatase inhibitor cocktails (Roche). Lysates were clarified by centrifugation for 10 min at 12,000 rpm at 4°C and precleared with Dynabeads (M280; Invitrogen) for 1 h at 4°C. Complexes were captured with anti-$\alpha_v$ integrin–conjugated (AB1930, Millipore) and BSA-blocked Dynabeads for 2 h at 4°C. Beads were washed in lysis buffer, and proteins were eluted in sample buffer (2× Laemmli). Cultured cells directly lysed in Laemmli buffer or bead-associated adhesion complexes were heat-denatured at 95°C for 5 min. Proteins were separated by SDS-PAGE, transferred to nitrocellulose membrane, and blotted with primary antibodies for Thy-1 (1:1,000, rabbit, 9798; Cell Signaling Technology), mouse Thy-1.2 (1:2,500, rat, 53-2.1; BD), $\alpha_v$ integrin (1:1,000, rabbit, AB1930; Millipore), $\alpha_5$ integrin (1:1,000, rabbit, AB1928; Millipore), talin (1:800, mouse, 8d4; Sigma-Aldrich), paxillin (1:1,000, mouse, 5H11; Millipore), pY397-FAK (1:1,000, rabbit, 44-624G; Invitrogen), Fyn (1:1,000, mouse, 1S; Millipore), c-Src (1:1,000, rabbit, 32G6; Cell Signaling Technology), pY418-SFK (1:1,000, rabbit, 2101; or 1:1,000, rabbit, D49G4; Cell Signaling Technology), flottilin-2 (1:1,000, rabbit, L294; Cell Signaling Technology), and Cbp (1:800, mouse, PAG-C1; Pierce Chemical). Two primary antibodies per membrane were detected using complementary secondary probes with distinct wavelengths for infrared detection (IRDye 680LT and 800CW; LI-COR). Signal was acquired using the Odyssey Infrared Imaging System (LI-COR). Membranes were not stripped and reprobed for multiple markers. Band intensity was quantified using ImageJ (National Institutes of Health) gel analyzer tools, and biological and technical replicates were pooled for statistical analysis.

## RhoA activity assay

RFL-6 or CCL-210 cells were plated on FN-PA substrates at $8 \times 10^3$/cm$^2$. After 4 h, cells were washed once with ice-cold PBS and the RhoA G-LISA assay (Cytoskeleton) was performed per the manufacturer's instructions. After absorbance measurements were taken at 490 nm, buffer-only background levels were subtracted and normalized by the experimental group with the lowest RhoA activity levels. For magnetic force application assays, cells were plated and subject to force application as described above and RhoA G-LISA was performed; relative RhoA activity values were obtained after normalizing to zero force RhoA activity signal per experimental group. Western blot for total RhoA protein was used to ensure protein expression of RhoA was equivalent between samples and treatment conditions.

## Inhibitor treatments

CholOx from *Streptomyces* species (Sigma-Aldrich) was used at a concentration of 1 U/ml. Cells were treated for 1 h before the start of magnetic tweezing and complex precipitation assays, and CholOx was maintained in the media during assays. 5 mM methyl-B-cyclodextrin (Sigma-Aldrich) was added for 1 h before fixation. 10 μM Y-27632 (Calbiochem) was added to spread cells on FN-PA substrates 2 h after plating and fixed after an additional 2 h. For collagen gel contraction experiments, Y-27632 was added after initial gelation and additional media supplementation. For integrin blocking experiments, cells were incubated with 10 μg/ml of function-blocking $\alpha_v$ (H9.2B8; Santa Cruz Biotechnology) or $\beta_3$ (2C9.G2; BioLegend) antibody in suspension for 30 min at 37°C, before being plated on FN-PA substrates in the presence of blocking antibodies, fixed. Cells were cultured for 2 h on soft FN-PA substrates and then treated with 0.5 mM cyclo-RGD/EfK (Anaspec) or 10 μM PP2 or PP3 (Calbiochem) for small molecule inhibitor experiments.

## Proximity ligation assays

Cells on No. 1.5 coverglass were fixed with 4% formaldehyde with 0.2% glutaraldehyde for 15 min at 25°C and blocked with 5% normal goat serum with 0.1% Tween-20. Primary antibodies used were for Thy-1 (1:1,000, EPR3132; Abcam), $\alpha_v\beta_3$ integrin (1:1,000, 23C6; Millipore), $\alpha_v\beta_3$ integrin (1:1,000, LM609; Millipore), LIBS2 epitope $\beta_3$ integrin (1:1,000, ab62; Millipore), $\alpha_v\beta_3$ integrin (1 μg/ml; WOW-1), $\beta_1$ integrin (1:1,500, K20; BD), $\beta_1$ integrin (1:1,000, HUTS-4; Millipore), and $\alpha_5$ (1:1,000, P1D6; Millipore). 2 mM Mn$^{2+}$ or 10 μg/ml LIBS2 was added to cultures for 1 h before fixation and PLA assays. For GFP-tagged THD constructs, remaining GFP fluorescence after fixation was bleached with a 488-nm laser, and the Alexa Fluor 488 immunofluorescence signal was collected. Proximity ligation assays were performed according to the manufacturer's instructions (Olink Biosciences).

## Cell spreading assays

Cells were trypsinized, resuspended in soybean trypsin inhibitor (Sigma-Aldrich), and held in suspension in DMEM for 30 min at 37°C. Cells were plated on FN-gl (10 μg/ml) and fixed and stained at various time points for confocal microscopy. For cell spreading dynamics, cells were stained in suspension with DiI (Invitrogen) and imaged by time-lapse epifluorescence and differential interference contrast microscopy every 10 s under 5% $CO_2$ and 37°C conditions. Cell area was quantified using the fluorescent DiI signal.

## Proliferation and apoptosis assays

Human LFs were cultured on soft (1.8 kPa) or stiff (18.7 kPa) FN-PA substrates for 3 d and then exposed to 50 µM BrdU for 24 additional hours and costained with Hoechst (33258, Invitrogen) for nuclear BrdU incorporation following the manufacturer's instructions (Exalpha Biologicals). Anti-BrdU was detected using anti–mouse Alexa Fluor 488 secondary antibody (Invitrogen). For apoptosis detection, cells were stained for caspase-3/7 activity after 4 d using the Image-iT Live Green Caspase Detection kit (Invitrogen). For quantification, micrographs were judged in a blinded manner for the total number of cells and the number of cells positive for nuclear BrdU or caspase-3/7 signal.

## FN assembly assays

Cells were plated onto FN-PA as described for immunofluorescence. To assay for DOC-insoluble matrix, cells were cultured in normal growth medium for 24 h and lysed in DOC lysis buffer (2% DOC, 20 mM Tris-HCl, pH 8.8, 2 mM EDTA, and cOmplete Protease Inhibitors). The DOC-insoluble fraction was isolated via centrifugation and solubilized in 1% SDS, 20 mM Tris-HCl, pH 8.8, 2 mM EDTA, and cOmplete Protease Inhibitors. Total protein concentrations were determined using the Quant-iT protein kit (Invitrogen), and equal amounts of DOC-soluble or the equivalent proportion of DOC-insoluble material were loaded for SDS-PAGE. Samples were blotted for FN (1:2,500, AB1930; Millipore) and GAPDH (1:2,000, ab9485; Abcam), and FN band intensity was measured and normalized to GAPDH. For labeled FN assembly, cells were cultured in serum depleted of endogenous FN and supplemented in 50 µg/ml AlexaFluor-488 labeled human plasma FN. After 24 h, samples were fixed and prepared for immunofluorescence imaging.

## Collagen gel contraction

Trypsinized cells were resuspended at $5 \times 10^6$ cells/ml in growth media and added to NaOH-neutralized acid-prepared rat tail type I collagen (BD) at a final suspension of $0.5 \times 10^5$ cells/ml in 1.7 mg/ml type I collagen. After polymerization for 60 min at 37°C, gels were disassociated and growth media was added to monitor floating contraction over 72 h. To obtain gel contraction values, the diameter of the well and the gel were measured using ImageJ, and the percentage of contraction was calculated using the formula 100 × (well diameter − gel diameter)/well diameter.

## Online supplemental material

Fig. S1 shows cell spreading responses in Thy-1 fibroblast subpopulations as a function of substrate rigidity and cell stiffness. Fig. S2 shows rigidity-dependent cell spreading responses for c-Src versus Fyn SFK family members, effects of CholOx on RhoA activation, and total cell surface staining of GM1. Fig. S3 shows the PLA responses using multiple integrin subunit-specific mAbs. Fig. S4 shows the Thy-1 dependence of adhesion rate to FN as a result of RGD inhibition and cell spreading and morphological dynamics on FN-gl. Fig. S5 shows Thy-1 expression in human fibroblast isolations for normal and IPF samples, their cytoskeletal and FN assembly phenotypes on soft and stiff FN-PA substrates, and shRNA knockdown efficiency and rescue experiments. Online supplemental material is available at http://www.jcb.org/cgi/content/full/jcb.201505007/DC1.

## References

Arias-Salgado, E.G., S. Lizano, S. Sarkar, J.S. Brugge, M.H. Ginsberg, and S.J. Shattil. 2003. Src kinase activation by direct interaction with the integrin beta cytoplasmic domain. *Proc. Natl. Acad. Sci. USA.* 100:13298–13302. http://dx.doi.org/10.1073/pnas.2336149100

Arias-Salgado, E.G., S. Lizano, S.J. Shattil, and M.H. Ginsberg. 2005. Specification of the direction of adhesive signaling by the integrin beta cytoplasmic domain. *J. Biol. Chem.* 280:29699–29707. http://dx.doi.org/10.1074/jbc.M503508200

Arthur, W.T., and K. Burridge. 2001. RhoA inactivation by p190RhoGAP regulates cell spreading and migration by promoting membrane protrusion and polarity. *Mol. Biol. Cell.* 12:2711–2720. http://dx.doi.org/10.1091/mbc.12.9.2711

Arthur, W.T., L.A. Petch, and K. Burridge. 2000. Integrin engagement suppresses RhoA activity via a c-Src-dependent mechanism. *Curr. Biol.* 10:719–722. http://dx.doi.org/10.1016/S0960-9822(00)00537-6

Barboni, E., B.P. Rivero, A.J. George, S.R. Martin, D.V. Renoup, E.F. Hounsell, P.C. Barber, and R.J. Morris. 1995. The glycophosphatidylinositol anchor affects the conformation of Thy-1 protein. *J. Cell Sci.* 108:487–497.

Barker, T.H., and J.S. Hagood. 2009. Getting a grip on Thy-1 signaling. *Biochim. Biophys. Acta.* 1793:921–923. http://dx.doi.org/10.1016/j.bbamcr.2008.10.004

Barker, T.H., H.E. Grenett, M.W. MacEwen, S.G. Tilden, G.M. Fuller, J. Settleman, A. Woods, J. Murphy-Ullrich, and J.S. Hagood. 2004a. Thy-1 regulates fibroblast focal adhesions, cytoskeletal organization and migration through modulation of p190 RhoGAP and Rho GTPase activity. *Exp. Cell Res.* 295:488–496. http://dx.doi.org/10.1016/j.yexcr.2004.01.026

Barker, T.H., M.A. Pallero, M.W. MacEwen, S.G. Tilden, A. Woods, J.E. Murphy-Ullrich, and J.S. Hagood. 2004b. Thrombospondin-1-induced focal adhesion disassembly in fibroblasts requires Thy-1 surface expression, lipid raft integrity, and Src activation. *J. Biol. Chem.* 279:23510–23516. http://dx.doi.org/10.1074/jbc.M402169200

Boettiger, D. 2012. Mechanical control of integrin-mediated adhesion and signaling. *Curr. Opin. Cell Biol.* 24:592–599. http://dx.doi.org/10.1016/j.ceb.2012.07.002

Booth, A.J., R. Hadley, A.M. Cornett, A.A. Dreffs, S.A. Matthes, J.L. Tsui, K. Weiss, J.C. Horowitz, V.F. Fiore, T.H. Barker, et al. 2012. Acellular normal and fibrotic human lung matrices as a culture system for in vitro investigation. *Am. J. Respir. Crit. Care Med.* 186:866–876. http://dx.doi.org/10.1164/rccm.201204-0754OC

Bouaouina, M., Y. Lad, and D.A. Calderwood. 2008. The N-terminal domains of talin cooperate with the phosphotyrosine binding-like domain to activate beta1 and beta3 integrins. *J. Biol. Chem.* 283:6118–6125. http://dx.doi.org/10.1074/jbc.M709527200

Bradley, J.E., J.M. Chan, and J.S. Hagood. 2013. Effect of the GPI anchor of human Thy-1 on antibody recognition and function. *Lab. Invest.* 93:365–374. http://dx.doi.org/10.1038/labinvest.2012.178

Brown, E.J., and W.A. Frazier. 2001. Integrin-associated protein (CD47) and its ligands. *Trends Cell Biol.* 11:130–135. http://dx.doi.org/10.1016/S0962-8924(00)01906-1

Brown, M.T., and J.A. Cooper. 1996. Regulation, substrates and functions of src. *Biochim. Biophys. Acta.* 1287:121–149.

Brown, A.C., V.F. Fiore, T.A. Sulchek, and T.H. Barker. 2013. Physical and chemical microenvironmental cues orthogonally control the degree and duration of fibrosis-associated epithelial-to-mesenchymal transitions. *J. Pathol.* 229:25–35. http://dx.doi.org/10.1002/path.4114

Bryksin, A.V., and I. Matsumura. 2010. Overlap extension PCR cloning: a simple and reliable way to create recombinant plasmids. *Biotechniques.* 48:463–465. http://dx.doi.org/10.2144/000113418

Butcher, D.T., T. Alliston, and V.M. Weaver. 2009. A tense situation: forcing tumour progression. *Nat. Rev. Cancer.* 9:108–122. http://dx.doi.org/10.1038/nrc2544

Byron, A., J.D. Humphries, J.A. Askari, S.E. Craig, A.P. Mould, and M.J. Humphries. 2009. Anti-integrin monoclonal antibodies. *J. Cell Sci.* 122:4009–4011. http://dx.doi.org/10.1242/jcs.056770

Calvo, F., N. Ege, A. Grande-Garcia, S. Hooper, R.P. Jenkins, S.I. Chaudhry, K. Harrington, P. Williamson, E. Moeendarbary, G. Charras, and E. Sahai. 2013. Mechanotransduction and YAP-dependent matrix remodelling is required for the generation and maintenance of cancer-associated fibroblasts. *Nat. Cell Biol.* 15:637–646. http://dx.doi.org/10.1038/ncb2756

Carraher, C.L., and J.E. Schwarzbauer. 2013. Regulation of matrix assembly through rigidity-dependent fibronectin conformational changes. *J. Biol. Chem.* 288:14805–14814. http://dx.doi.org/10.1074/jbc.M112.435271

Chang, H.Y., J.T. Chi, S. Dudoit, C. Bondre, M. van de Rijn, D. Botstein, and P.O. Brown. 2002. Diversity, topographic differentiation, and positional memory in human fibroblasts. *Proc. Natl. Acad. Sci. USA.* 99:12877–12882. http://dx.doi.org/10.1073/pnas.162488599

Chen, Y., W.R. Thelin, B. Yang, S.L. Milgram, and K. Jacobson. 2006. Transient anchorage of cross-linked glycosyl-phosphatidylinositol-anchored proteins depends on cholesterol, Src family kinases, caveolin, and phosphoinositides. *J. Cell Biol.* 175:169–178. http://dx.doi.org/10.1083/jcb.200512116

Chen, Y., L. Veracini, C. Benistant, and K. Jacobson. 2009. The transmembrane protein CBP plays a role in transiently anchoring small clusters of Thy-1, a GPI-anchored protein, to the cytoskeleton. *J. Cell Sci.* 122:3966–3972. http://dx.doi.org/10.1242/jcs.049346

Cool, C.D., S.D. Groshong, P.R. Rai, P.M. Henson, J.S. Stewart, and K.K. Brown. 2006. Fibroblast foci are not discrete sites of lung injury or repair: the fibroblast reticulum. *Am. J. Respir. Crit. Care Med.* 174:654–658. http://dx.doi.org/10.1164/rccm.200602-205OC

del Pozo, M.A., N.B. Alderson, W.B. Kiosses, H.H. Chiang, R.G. Anderson, and M.A. Schwartz. 2004. Integrins regulate Rac targeting by internalization of membrane domains. *Science.* 303:839–842. http://dx.doi.org/10.1126/science.1092571

Dráberová, L., and P. Dráber. 1993. Thy-1 glycoprotein and src-like protein-tyrosine kinase p53/p56lyn are associated in large detergent-resistant complexes in rat basophilic leukemia cells. *Proc. Natl. Acad. Sci. USA.* 90:3611–3615. http://dx.doi.org/10.1073/pnas.90.8.3611

Du, X., M. Gu, J.W. Weisel, C. Nagaswami, J.S. Bennett, R. Bowditch, and M.H. Ginsberg. 1993. Long range propagation of conformational changes in integrin alpha IIb beta 3. *J. Biol. Chem.* 268:23087–23092.

Duband, J.L., G.H. Nuckolls, A. Ishihara, T. Hasegawa, K.M. Yamada, J.P. Thiery, and K. Jacobson. 1988. Fibronectin receptor exhibits high lateral mobility in embryonic locomoting cells but is immobile in focal contacts and fibrillar streaks in stationary cells. *J. Cell Biol.* 107:1385–1396. http://dx.doi.org/10.1083/jcb.107.4.1385

Dubin-Thaler, B.J., G. Giannone, H.G. Döbereiner, and M.P. Sheetz. 2004. Nanometer analysis of cell spreading on matrix-coated surfaces reveals two distinct cell states and STEPs. *Biophys. J.* 86:1794–1806. http://dx.doi.org/10.1016/S0006-3495(04)74246-0

Fiore, V.F., L. Ju, Y. Chen, C. Zhu, and T.H. Barker. 2014. Dynamic catch of a Thy-1–α5β1+syndecan-4 trimolecular complex. *Nat. Commun.* 5:4886. http://dx.doi.org/10.1038/ncomms5886

Friedland, J.C., M.H. Lee, and D. Boettiger. 2009. Mechanically activated integrin switch controls alpha5beta1 function. *Science.* 323:642–644. http://dx.doi.org/10.1126/science.1168441

Friedrichs, J., J. Helenius, and D.J. Muller. 2010. Quantifying cellular adhesion to extracellular matrix components by single-cell force spectroscopy. *Nat. Protoc.* 5:1353–1361. http://dx.doi.org/10.1038/nprot.2010.89

Gaus, K., S. Le Lay, N. Balasubramanian, and M.A. Schwartz. 2006. Integrin-mediated adhesion regulates membrane order. *J. Cell Biol.* 174:725–734. http://dx.doi.org/10.1083/jcb.200603034

Georges, P.C., J.J. Hui, Z. Gombos, M.E. McCormick, A.Y. Wang, M. Uemura, R. Mick, P.A. Janmey, E.E. Furth, and R.G. Wells. 2007. Increased stiffness of the rat liver precedes matrix deposition: implications for fibrosis. *Am. J. Physiol. Gastrointest. Liver Physiol.* 293:G1147–G1154. http://dx.doi.org/10.1152/ajpgi.00032.2007

Giannone, G., B.J. Dubin-Thaler, H.G. Döbereiner, N. Kieffer, A.R. Bresnick, and M.P. Sheetz. 2004. Periodic lamellipodial contractions correlate with rearward actin waves. *Cell.* 116:431–443. http://dx.doi.org/10.1016/S0092-8674(04)00058-3

Goetz, J.G., S. Minguet, I. Navarro-Lérida, J.J. Lazcano, R. Samaniego, E. Calvo, M. Tello, T. Osteso-Ibáñez, T. Pellinen, A. Echarri, et al. 2011. Biomechanical remodeling of the microenvironment by stromal caveolin-1 favors tumor invasion and metastasis. *Cell.* 146:148–163. http://dx.doi.org/10.1016/j.cell.2011.05.040

Goffin, J.M., P. Pittet, G. Csucs, J.W. Lussi, J.J. Meister, and B. Hinz. 2006. Focal adhesion size controls tension-dependent recruitment of alpha-smooth muscle actin to stress fibers. *J. Cell Biol.* 172:259–268. http://dx.doi.org/10.1083/jcb.200506179

Guilluy, C., V. Swaminathan, R. Garcia-Mata, E.T. O'Brien, R. Superfine, and K. Burridge. 2011. The Rho GEFs LARG and GEF-H1 regulate the mechanical response to force on integrins. *Nat. Cell Biol.* 13:722–727. http://dx.doi.org/10.1038/ncb2254

Hagood, J.S., P. Prabhakaran, P. Kumbla, L. Salazar, M.W. MacEwen, T.H. Barker, L.A. Ortiz, T. Schoeb, G.P. Siegal, C.B. Alexander, et al. 2005. Loss of fibroblast Thy-1 expression correlates with lung fibrogenesis. *Am. J. Pathol.* 167:365–379. http://dx.doi.org/10.1016/S0002-9440(10)62982-3

Hardie, W.D., S.W. Glasser, and J.S. Hagood. 2009. Emerging concepts in the pathogenesis of lung fibrosis. *Am. J. Pathol.* 175:3–16. http://dx.doi.org/10.2353/ajpath.2009.081170

Hermosilla, T., D. Muñoz, R. Herrera-Molina, A. Valdivia, N. Muñoz, S.U. Nham, P. Schneider, K. Burridge, A.F. Quest, and L. Leyton. 2008. Direct Thy-1/alphaVbeta3 integrin interaction mediates neuron to astrocyte communication. *Biochim. Biophys. Acta.* 1783:1111–1120. http://dx.doi.org/10.1016/j.bbamcr.2008.01.034

Hoffman, B.D., C. Grashoff, and M.A. Schwartz. 2011. Dynamic molecular processes mediate cellular mechanotransduction. *Nature.* 475:316–323. http://dx.doi.org/10.1038/nature10316

Huang, X., N. Yang, V.F. Fiore, T.H. Barker, Y. Sun, S.W. Morris, Q. Ding, V.J. Thannickal, and Y. Zhou. 2012. Matrix stiffness-induced myofibroblast differentiation is mediated by intrinsic mechanotransduction. *Am. J. Respir. Cell Mol. Biol.* 47:340–348. http://dx.doi.org/10.1165/rcmb.2012-0050OC

Iskratsch, T., C.H. Yu, A. Mathur, S. Liu, V. Stévenin, J. Dwyer, J. Hone, E. Ehler, and M. Sheetz. 2013. FHOD1 is needed for directed forces and adhesion maturation during cell spreading and migration. *Dev. Cell.* 27:545–559. http://dx.doi.org/10.1016/j.devcel.2013.11.003

King, T.E. Jr., M.I. Schwarz, K. Brown, J.A. Tooze, T.V. Colby, J.A. Waldron Jr., A. Flint, W. Thurlbeck, and R.M. Cherniack. 2001. Idiopathic pulmonary fibrosis: relationship between histopathologic features and mortality. *Am. J. Respir. Crit. Care Med.* 164:1025–1032. http://dx.doi.org/10.1164/ajrccm.164.6.2001056

Klinghoffer, R.A., C. Sachsenmaier, J.A. Cooper, and P. Soriano. 1999. Src family kinases are required for integrin but not PDGFR signal transduction. *EMBO J.* 18:2459–2471. http://dx.doi.org/10.1093/emboj/18.9.2459

Kostic, A., and M.P. Sheetz. 2006. Fibronectin rigidity response through Fyn and p130Cas recruitment to the leading edge. *Mol. Biol. Cell.* 17:2684–2695. http://dx.doi.org/10.1091/mbc.E05-12-1161

Legate, K.R., and R. Fässler. 2009. Mechanisms that regulate adaptor binding to beta-integrin cytoplasmic tails. *J. Cell Sci.* 122:187–198. http://dx.doi.org/10.1242/jcs.041624

Leitinger, B., and N. Hogg. 2002. The involvement of lipid rafts in the regulation of integrin function. *J. Cell Sci.* 115:963–972.

Leyton, L., P. Schneider, C.V. Labra, C. Rüegg, C.A. Hetz, A.F. Quest, and C. Bron. 2001. Thy-1 binds to integrin beta(3) on astrocytes and triggers formation of focal contact sites. *Curr. Biol.* 11:1028–1038. http://dx.doi.org/10.1016/S0960-9822(01)00262-7

Lin, E.C., C.P. Carron, D.M. Meyer, and J.W. Smith. 1998. A series of function blocking antibodies against the αvβ3 integrin bind allosteric to the ligand binding site and induce ligand dissociation. *Cell Adhes. Commun.* 6:451–464. http://dx.doi.org/10.3109/15419069809010794

Lindberg, F.P., H.D. Gresham, M.I. Reinhold, and E.J. Brown. 1996. Integrin-associated protein immunoglobulin domain is necessary for efficient vitronectin bead binding. *J. Cell Biol.* 134:1313–1322. http://dx.doi.org/10.1083/jcb.134.5.1313

Liu, F., J.D. Mih, B.S. Shea, A.T. Kho, A.S. Sharif, A.M. Tager, and D.J. Tschumperlin. 2010. Feedback amplification of fibrosis through matrix stiffening and COX-2 suppression. *J. Cell Biol.* 190:693–706. http://dx.doi.org/10.1083/jcb.20100408220733059

Luo, B.H., C.V. Carman, and T.A. Springer. 2007. Structural basis of integrin regulation and signaling. *Annu. Rev. Immunol.* 25:619–647. http://dx.doi.org/10.1146/annurev.immunol.25.022106.141618

Markowski, M.C., A.C. Brown, and T.H. Barker. 2012. Directing epithelial to mesenchymal transition through engineered microenvironments displaying orthogonal adhesive and mechanical cues. *J. Biomed. Mater. Res. A.* 100:2119–2127. http://dx.doi.org/10.1002/jbm.a.34068

McIntosh, J.C., J.S. Hagood, T.L. Richardson, and J.W. Simecka. 1994. Thy1 (+) and (-) lung fibrosis subpopulations in LEW and F344 rats. *Eur. Respir. J.* 7:2131–2138. http://dx.doi.org/10.1183/09031936.94.07122131

Nicholson, A.G., L.G. Fulford, T.V. Colby, R.M. du Bois, D.M. Hansell, and A.U. Wells. 2002. The relationship between individual histologic features and disease progression in idiopathic pulmonary fibrosis. *Am. J. Respir. Crit. Care Med.* 166:173–177. http://dx.doi.org/10.1164/rccm.2109039

Norambuena, A., and M.A. Schwartz. 2011. Effects of integrin-mediated cell adhesion on plasma membrane lipid raft components and signaling. *Mol. Biol. Cell.* 22:3456–3464. http://dx.doi.org/10.1091/mbc.E11-04-0361

Palazzo, A.F., C.H. Eng, D.D. Schlaepfer, E.E. Marcantonio, and G.G. Gundersen. 2004. Localized stabilization of microtubules by integrin- and FAK-facilitated Rho signaling. *Science.* 303:836–839. http://dx.doi.org/10.1126/science.1091325

Pampori, N., T. Hato, D.G. Stupack, S. Aidoudi, D.A. Cheresh, G.R. Nemerow, and S.J. Shattil. 1999. Mechanisms and consequences of affinity modulation of integrin alpha(V)beta(3) detected with a novel patch-engineered monovalent ligand. *J. Biol. Chem.* 274:21609–21616. http://dx.doi.org/10.1074/jbc.274.31.21609

Paszek, M.J., D. Boettiger, V.M. Weaver, and D.A. Hammer. 2009. Integrin clustering is driven by mechanical resistance from the glycocalyx and the substrate. *PLOS Comput. Biol.* 5:e1000604. http://dx.doi.org/10.1371/journal.pcbi.1000604

Paszek, M.J., C.C. DuFort, O. Rossier, R. Bainer, J.K. Mouw, K. Godula, J.E. Hudak, J.N. Lakins, A.C. Wijekoon, L. Cassereau, et al. 2014. The cancer glycocalyx mechanically primes integrin-mediated growth and survival. *Nature.* 511:319–325. http://dx.doi.org/10.1038/nature13535

Pelham, R.J. Jr., and Y. Wang. 1997. Cell locomotion and focal adhesions are regulated by substrate flexibility. *Proc. Natl. Acad. Sci. USA.* 94:13661–13665. http://dx.doi.org/10.1073/pnas.94.25.13661

Pierschbacher, M.D., and E. Ruoslahti. 1987. Influence of stereochemistry of the sequence Arg-Gly-Asp-Xaa on binding specificity in cell adhesion. *J. Biol. Chem.* 262:17294–17298.

Reddy, K.B., D.M. Smith, and E.F. Plow. 2008. Analysis of Fyn function in hemostasis and αIIbβ3-integrin signaling. *J. Cell Sci.* 121:1641–1648. http://dx.doi.org/10.1242/jcs.014076

Rege, T.A., M.A. Pallero, C. Gomez, H.E. Grenett, J.E. Murphy-Ullrich, and J.S. Hagood. 2006. Thy-1, via its GPI anchor, modulates Src family kinase and focal adhesion kinase phosphorylation and subcellular localization, and fibroblast migration, in response to thrombospondin-1/hep I. *Exp. Cell Res.* 312:3752–3767. http://dx.doi.org/10.1016/j.yexcr.2006.07.029

Rossier, O., V. Octeau, J.B. Sibarita, C. Leduc, B. Tessier, D. Nair, V. Gatterdam, O. Destaing, C. Albigès-Rizo, R. Tampé, et al. 2012. Integrins β1 and β3 exhibit distinct dynamic nanoscale organizations inside focal adhesions. *Nat. Cell Biol.* 14:1057–1067. http://dx.doi.org/10.1038/ncb2588

Saalbach, A., A. Wetzel, U.F. Haustein, M. Sticherling, J.C. Simon, and U. Anderegg. 2005. Interaction of human Thy-1 (CD 90) with the integrin alphavbeta3 (CD51/CD61): an important mechanism mediating melanoma cell adhesion to activated endothelium. *Oncogene.* 24:4710–4720. http://dx.doi.org/10.1038/sj.onc.1208559

Samaniego, R., A. Estecha, M. Relloso, N. Longo, J.L. Escat, I. Longo-Imedio, J.A. Avilés, M.A. del Pozo, A. Puig-Kröger, and P. Sánchez-Mateos. 2013. Mesenchymal contribution to recruitment, infiltration, and positioning of leukocytes in human melanoma tissues. *J. Invest. Dermatol.* 133:2255–2264. http://dx.doi.org/10.1038/jid.2013.88

Sanders, Y.Y., A. Pardo, M. Selman, G.J. Nuovo, T.O. Tollefsbol, G.P. Siegal, and J.S. Hagood. 2008. Thy-1 promoter hypermethylation: a novel epigenetic pathogenic mechanism in pulmonary fibrosis. *Am. J. Respir. Cell Mol. Biol.* 39:610–618. http://dx.doi.org/10.1165/rcmb.2007-0322OC

Sandilands, E., V.G. Brunton, and M.C. Frame. 2007. The membrane targeting and spatial activation of Src, Yes and Fyn is influenced by palmitoylation and distinct RhoB/RhoD endosome requirements. *J. Cell Sci.* 120:2555–2564. http://dx.doi.org/10.1242/jcs.003657

Shattil, S.J. 2005. Integrins and Src: dynamic duo of adhesion signaling. *Trends Cell Biol.* 15:399–403. http://dx.doi.org/10.1016/j.tcb.2005.06.005

Shima, T., S. Nada, and M. Okada. 2003. Transmembrane phosphoprotein Cbp senses cell adhesion signaling mediated by Src family kinase in lipid rafts. *Proc. Natl. Acad. Sci. USA.* 100:14897–14902. http://dx.doi.org/10.1073/pnas.2432139100

Solon, J., I. Levental, K. Sengupta, P.C. Georges, and P.A. Janmey. 2007. Fibroblast adaptation and stiffness matching to soft elastic substrates. *Biophys. J.* 93:4453–4461. http://dx.doi.org/10.1529/biophysj.106.101386

Sorrell, J.M., and A.I. Caplan. 2004. Fibroblast heterogeneity: more than skin deep. *J. Cell Sci.* 117:667–675. http://dx.doi.org/10.1242/jcs.01005

Sorrell, J.M., and A.I. Caplan. 2009. Fibroblasts-a diverse population at the center of it all. *Int. Rev. Cell Mol. Biol.* 276:161–214. http://dx.doi.org/10.1016/S1937-6448(09)76004-6

Stefanová, I., V. Horejsí, I.J. Ansotegui, W. Knapp, and H. Stockinger. 1991. GPI-anchored cell-surface molecules complexed to protein tyrosine kinases. *Science.* 254:1016–1019. http://dx.doi.org/10.1126/science.1719635

Sueblinvong, V., D.C. Neujahr, S.T. Mills, S. Roser-Page, J.D. Ritzenthaler, D. Guidot, M. Rojas, and J. Roman. 2012. Predisposition for disrepair in the aged lung. *Am. J. Med. Sci.* 344:41–51. http://dx.doi.org/10.1097/MAJ.0b013e318234c132

Takagi, J., B.M. Petre, T. Walz, and T.A. Springer. 2002. Global conformational rearrangements in integrin extracellular domains in outside-in and inside-out signaling. *Cell.* 110:599–611. http://dx.doi.org/10.1016/S0092-8674(02)00935-2

Thomas, S.M., and J.S. Brugge. 1997. Cellular functions regulated by Src family kinases. *Annu. Rev. Cell Dev. Biol.* 13:513–609. http://dx.doi.org/10.1146/annurev.cellbio.13.1.513

Tiveron, M.C., M. Nosten-Bertrand, H. Jani, D. Garnett, E.M. Hirst, F. Grosveld, and R.J. Morris. 1994. The mode of anchorage to the cell surface determines both the function and the membrane location of Thy-1 glycoprotein. *J. Cell Sci.* 107:1783–1796.

Tomasek, J.J., G. Gabbiani, B. Hinz, C. Chaponnier, and R.A. Brown. 2002. Myofibroblasts and mechano-regulation of connective tissue remodelling. *Nat. Rev. Mol. Cell Biol.* 3:349–363. http://dx.doi.org/10.1038/nrm809

True, L.D., H. Zhang, M. Ye, C.Y. Huang, P.S. Nelson, P.D. von Haller, L.W. Tjoelker, J.S. Kim, W.J. Qian, R.D. Smith, et al. 2010. CD90/THY1 is overexpressed in prostate cancer-associated fibroblasts and could serve as a cancer biomarker. *Mod. Pathol.* 23:1346–1356.

van Zanten, T.S., A. Cambi, M. Koopman, B. Joosten, C.G. Figdor, and M.F. Garcia-Parajo. 2009. Hotspots of GPI-anchored proteins and integrin nanoclusters function as nucleation sites for cell adhesion. *Proc. Natl. Acad. Sci. USA.* 106:18557–18562. http://dx.doi.org/10.1073/pnas.0905217106

Visscher, D.W., and J.L. Myers. 2006. Histologic spectrum of idiopathic interstitial pneumonias. *Proc. Am. Thorac. Soc.* 3:322–329. http://dx.doi.org/10.1513/pats.200602-019TK

von Wichert, G., G. Jiang, A. Kostic, K. De Vos, J. Sap, and M.P. Sheetz. 2003. RPTP-alpha acts as a transducer of mechanical force on alphav/beta3-integrin-cytoskeleton linkages. *J. Cell Biol.* 161:143–153. http://dx.doi.org/10.1083/jcb.200211061

Watanabe, T., and F. Sendo. 2002. Physical association of beta 2 integrin with GPI-80, a novel glycosylphosphatidylinositol-anchored protein with potential for regulating adhesion and migration. *Biochem. Biophys. Res. Commun.* 294:692–694. http://dx.doi.org/10.1016/S0006-291X(02)00538-7

Wei, Y., M. Lukashev, D.I. Simon, S.C. Bodary, S. Rosenberg, M.V. Doyle, and H.A. Chapman. 1996. Regulation of integrin function by the urokinase receptor. *Science.* 273:1551–1555. http://dx.doi.org/10.1126/science.273.5281.1551

Wei, Y., R.P. Czekay, L. Robillard, M.C. Kugler, F. Zhang, K.K. Kim, J.P. Xiong, M.J. Humphries, and H.A. Chapman. 2005. Regulation of alpha5beta1 integrin conformation and function by urokinase receptor binding. *J. Cell Biol.* 168:501–511. http://dx.doi.org/10.1083/jcb.200404112

White, E.S., V.J. Thannickal, S.L. Carskadon, E.G. Dickie, D.L. Livant, S. Markwart, G.B. Toews, and D.A. Arenberg. 2003. Integrin α4β1 regulates migration across basement membranes by lung fibroblasts: a role for phosphatase and tensin homologue deleted on chromosome 10. *Am. J. Respir. Crit. Care Med.* 168:436–442. http://dx.doi.org/10.1164/rccm.200301-041OC

Wipff, P.J., D.B. Rifkin, J.J. Meister, and B. Hinz. 2007. Myofibroblast contraction activates latent TGF-β1 from the extracellular matrix. *J. Cell Biol.* 179:1311–1323. http://dx.doi.org/10.1083/jcb.200704042

Wiseman, P.W., C.M. Brown, D.J. Webb, B. Hebert, N.L. Johnson, J.A. Squier, M.H. Ellisman, and A.F. Horwitz. 2004. Spatial mapping of integrin interactions and dynamics during cell migration by image correlation microscopy. *J. Cell Sci.* 117:5521–5534. http://dx.doi.org/10.1242/jcs.01416

Wolfenson, H., I. Lavelin, and B. Geiger. 2013. Dynamic regulation of the structure and functions of integrin adhesions. *Dev. Cell.* 24:447–458. http://dx.doi.org/10.1016/j.devcel.2013.02.012

Wolfenson, H., T. Iskratsch, and M.P. Sheetz. 2014. Early events in cell spreading as a model for quantitative analysis of biomechanical events. *Biophys. J.* 107:2508–2514. http://dx.doi.org/10.1016/j.bpj.2014.10.041

Xiong, J.P., T. Stehle, B. Diefenbach, R. Zhang, R. Dunker, D.L. Scott, A. Joachimiak, S.L. Goodman, and M.A. Arnaout. 2001. Crystal structure of the extracellular segment of integrin alpha Vbeta3. *Science.* 294:339–345. http://dx.doi.org/10.1126/science.1064535

Yeung, T., P.C. Georges, L.A. Flanagan, B. Marg, M. Ortiz, M. Funaki, N. Zahir, W. Ming, V. Weaver, and P.A. Janmey. 2005. Effects of substrate stiffness on cell morphology, cytoskeletal structure, and adhesion. *Cell Motil. Cytoskeleton.* 60:24–34. http://dx.doi.org/10.1002/cm.20041

Yoshitake, H., Y. Takeda, T. Nitto, F. Sendo, and Y. Araki. 2003. GPI-80, a beta2 integrin associated glycosylphosphatidylinositol-anchored protein, concentrates on pseudopodia without association with beta2 integrin during neutrophil migration. *Immunobiology.* 208:391–399. http://dx.doi.org/10.1078/0171-2985-00281

Zhou, Y., J.S. Hagood, B. Lu, W.D. Merryman, and J.E. Murphy-Ullrich. 2010. Thy-1-integrin αvβ5 interactions inhibit lung fibroblast contraction-induced latent transforming growth factor-beta1 activation and myofibroblast differentiation. *J. Biol. Chem.* 285:22382–22393. http://dx.doi.org/10.1074/jbc.M110.126227